PHYSICAL REVIEW D **81,** 095012 (2010)

Fitting the phenomenological MSSM

Shehu S. AbdusSalam,[1,*] Benjamin C. Allanach,[1,†] Fernando Quevedo,[1,2,‡] Farhan Feroz,[3,§] and Mike Hobson[3,‖]

[1]*DAMTP, Center for Mathematical Sciences, Wilberforce Road, Cambridge CB3 0WA, United Kingdom*

[2]*CERN, PH-TH, CH-1211, Geneva 23, Switzerland*

[3]*Cavendish Laboratory, JJ Thomson Avenue, Cambridge CB3 0HE, United Kingdom*

(Received 3 February 2010; published 20 May 2010)

We perform a global Bayesian fit of the phenomenological minimal supersymmetric standard model (pMSSM) to current indirect collider and dark matter data. The pMSSM contains the most relevant 25 weak-scale MSSM parameters, which are simultaneously fit using ''nested sampling'' Monte Carlo techniques in more than 15 years of CPU time. We calculate the Bayesian evidence for the pMSSM and constrain its parameters and observables in the context of two widely different, but reasonable, priors to determine which inferences are robust. We make inferences about sparticle masses, the sign of the μ parameter, the amount of fine-tuning, dark matter properties, and the prospects for direct dark matter detection without assuming a restrictive high-scale supersymmetry breaking model. We find the inferred lightest *CP*-even Higgs boson mass as an example of an approximately prior-independent observable. This analysis constitutes the first statistically convergent pMSSM global fit to all current data.

DOI: 10.1103/PhysRevD.81.095012 PACS numbers: 12.60.Jv

I. INTRODUCTION

There is currently an expectation that with the start of the Large Hadron Collider (LHC), high energy physics will soon enter a new phase highly dominated by new data that could imply physics beyond the standard model (SM). Over the past years, low-energy supersymmetry (SUSY) has become the standard approach to study the potential physics beyond the SM, mostly because of its natural power to address the hierarchy problem. The 124 Lagrangian parameters of the minimal supersymmetric extension of the SM (for a recent review, see [1]) makes its phenomenological study impractical. It may well be that the mechanism that mediates SUSY breaking to the observable sector provides relations between many of these parameters. Unfortunately, however, there are many different mediation mechanisms in the literature, with no one clearly preferred.

In order to extract computable information, many works have reduced the number of parameters by truncating to a handful of soft-breaking parameters at a high energy scale. The remaining set of parameters are used as boundary conditions for renormalization group equations (RGE), which are run down to the weak scale. A large number of minimal supersymmetric standard model (MSSM) based studies have been carried out in the way described above. Most of them were performed in the context of the constrained MSSM (CMSSM, also sometimes called mSUGRA for minimal supergravity) setup, which have only four independent non-SM parameters (and a sign choice). Many groups have been pursuing a program to fit this model and identify regions in parameter space that might be of interest with the forthcoming LHC data. See, for instance, [2–7]. Complete scans over up to eight free parameters of CMSSM with a combined treatment of likelihoods from different experimental constraints were possible with Markov chain Monte Carlo (MCMC) sampling techniques [5,8–14]. However, the truncation to a handful of parameters in the CMSSM is at best a very strong assumption, and most likely overrestrictive.

There are two directions that can be followed to properly study low-energy supersymmetric models. The top-down approach has been tried over the years by deriving the otherwise free parameters from an ultraviolet extension of the MSSM. Models of unification, different sources of SUSY breaking, such as gravity and gauge mediation, and classes of string compactifications [15–23] have been used to provide high energy expressions for the soft-breaking parameters. Soft SUSY-breaking terms can be computed at energies as high as the grand unified theory (GUT) scale of $\sim 10^{16}$ GeV, and renormalization group running to the TeV scale allows contact to be made with potential quantities of interest such as sparticle masses. Recent progress in moduli stabilization in string theory has made this approach more concrete and calculable with explicit results for some classes of models. This is very encouraging but usually the string derived models fill only a small subset of the full CMSSM parameter space, which could make them impossible to differentiate from the CMSSM. The proliferation of SUSY-breaking mechanism setups mean that analyses where only one is picked tend to be very specific, with a rather limited range of applicability. It is desirable to sidestep such extreme model dependence with a different approach.

Alternatively, one can use a bottom-up approach to low-energy SUSY. In this case the soft-breaking parameters are

*s.s.abdussalam@damtp.cam.ac.uk
†b.c.allanach@damtp.cam.ac.uk
‡f.quevedo@damtp.cam.ac.uk
§f.feroz@mrao.cam.ac.uk
‖mph@mrao.cam.ac.uk

 © 2010 The American Physical Society

considered at the SUSY scale without referring to their high energy origin. All the parameters can in principle be varied over the experimentally allowed range and compared with potential observations at the LHC and other experiments. It is a formidable task to consider all the 124 parameters, due mostly to computing limitations. An interesting compromise is the phenomenological MSSM (pMSSM) [24], which we consider here. In this model, the number of free parameters is 20 soft-breaking parameters (and a ± 1 parameter) plus 5 SM ones, and they are selected by the requirements of consistency with unobserved flavor changing and *CP* violating processes. However, even this simplified version of the MSSM requires a lot of computer power to be analyzed in and details. The ability of future collider measurements to constrain the pMSSM has been estimated using MCMC methods in Refs. [25,26].

At present, SUSY forecasts for the LHC necessarily contain large uncertainties. In particular, there is a strong model dependence on the mechanism for SUSY breaking. Realistic predictions need guidance from direct and precise (collider and other related) experimental data. Interestingly, the converse is also very important: the experiments need unbiased phenomenological guidance about the expected nature or properties of SUSY. This is what we aim to accomplish, eventually.

The purpose of this article is to perform a global fit of the pMSSM and make SUSY forecasts for collider and dark matter search experiments using Bayesian statistics methods. For given prior probability and likelihood densities, Bayes' theorem provides the way to extract the posterior probability density for the parameters. It can also be used for model comparison when enough data are available. This formalism has been used in many fields of science, including cosmology (see [27,28] for recent reviews). MCMC and related techniques have recently begun to be used to perform Bayesian inference on supersymmetric models. The increasing access to large scale computing power and improved methods of calculation are making these techniques more manageable with time, and we have been able to tackle the relevant parameters of the pMSSM.

The complete and simultaneous scan of the 25 parameters and a sign[1] for the pMSSM construction was performed using the MULTINEST program [29,30]. At the heart of the algorithm is the nested sampling technique [31] that revolutionized computational Bayesian inference by prioritizing a computation of the Bayesian evidence rather than solely on computing the posterior probability distribution function (PDF) of model parameters (although the latter is obtained at no additional cost), as is the case in traditional Monte Carlo algorithms (e.g. MCMC method). We will review the nested sampling method in the Appendix. In simple terms, similar to the MCMC method, nested sampling is an iterative Monte Carlo method that, starting with a relatively small number of points (a few thousand in our case), it produces a list of a large number of points (10^7–10^8 in our case) ordered in increasing likelihood. We used it here because it computes both the evidence *and* the posterior PDF, as opposed to traditional MCMC methods, which calculate only the posterior PDFs. Further, the MULTINEST algorithm is efficient in handling complicated problems with multimodal/degenerate posterior distributions.

We emphasize that the current situation with no direct sparticle measurement data yet from LHC makes the issue of prior dependence critical. For this reason, it is expected that extraction of prior-independent information of our analysis will be difficult. Interestingly, however, we find some results with approximate prior independence. In order to illustrate the issue of prior dependence of results, we consider priors that are flat in the parameters themselves (''linear'') and flat in the logarithm of the parameters (''log'') priors. As is usual in Bayesian statistics, prior dependence should not be understood as a drawback but as a positive feature that can be used to determine when enough data are available to unambiguously make inferences. It is expected that, if SUSY is discovered, the addition of LHC sparticle mass data will relax any prior dependence, and so an analysis along the lines of ours could be used to extract prior-independent information.

The amount of work related to this project required very efficient algorithms and access to high performance computing. We used the University of Cambridge supercomputers: COSMOS from the Department of Applied Mathematics and Theoretical Physics (DAMTP) and the *Darwin* cluster from the High Performance Computing Service (HPC). The final run was made in terms of 60 twelve-hour jobs, each corresponding to a cluster of 128 CPUs on HPC, and 40 eight-hour jobs, each corresponding to a cluster of 64 CPUs, on COSMOS (making a total of more than 15-year standard CPU time). Some results of complete and independent (from the one we present here) runs with fewer experimental constraints were presented by one of us (S. S. A) at the SUSY 2008 conference and reported in Ref. [32]. While we were upgrading our analysis, a study of randomly scanned pMSSM points appeared [33], similar in philosophy to Ref. [4]. In the conclusions, we contrast the aims and methodologies of our work with these.

In order to make a self-contained presentation, we briefly describe Bayesian inference and relevant terminologies in Sec. II. We construct the elements needed for inference in the context of the pMSSM in Sec. III. The experimental constraints or observables used are described in Sec. III B. The sampling procedure and the different high energy physics software used to predict the observables are presented in Sec. III D. In Secs. IV and V we

[1]Where we refer to 25 parameters, we shall really mean 25 continuously varying parameters plus the one discrete sign choice.

analyze our results and then conclude. In the Appendix we briefly review the nested sampling method and how the MULTINEST program works.

II. BAYESIAN INFERENCE

Bayesian inference fits and plays an important role in the scientific process of data collection and modeling. It particularly deals with the steps that involve model fitting to data and the technique of assigning preferences to alternative models (model comparison). This subject is very important especially with the imminent start of the LHC experiments. Here we will give a short review of the basics of Bayesian statistics that are useful in our work.

A. Bayes' theorem

Consider a given model or hypothesis H (we shall take H to be the pMSSM) defined by some set of parameters (in our case, 25 parameters) $\boldsymbol{\Theta}$. We wish to know the PDF $P(\boldsymbol{\Theta}|\mathbf{D}, H)$ of the parameters $\boldsymbol{\Theta}$ given the data $\mathbf{D}$ and the model setup H. $P(\boldsymbol{\Theta}|\mathbf{D}, H)$, being the parameters' PDF *after* confrontation with data, is called the *posterior* PDF. The likelihood, $P(\mathbf{D}|\boldsymbol{\Theta}, H) \equiv L(\boldsymbol{\Theta})$, is a measure of how well a model point $\boldsymbol{\Theta}$ predicts data set $\mathbf{D}$. In order to calculate the posterior from the likelihood, one must assign some *prior* PDF to the parameters $P(\boldsymbol{\Theta}|H) \equiv \pi(\boldsymbol{\Theta})$ to parametrize our uncertainty in them before the model is confronted with data. Bayes' theorem then describes how one may obtain the posterior from the other two PDFs and a normalization constant $P(\mathbf{D}|H) \equiv Z$, the *Bayesian evidence* for the model in light of the data:

$$P(\boldsymbol{\Theta}|\mathbf{D}, H) = \frac{P(\mathbf{D}|\boldsymbol{\Theta}, H)P(\boldsymbol{\Theta}|H)}{P(\mathbf{D}|H)} \equiv \frac{L(\boldsymbol{\Theta})\pi(\boldsymbol{\Theta})}{Z}. \quad (2.1)$$

The Bayesian evidence is given by

$$Z = \int L(\boldsymbol{\Theta})\pi(\boldsymbol{\Theta})d^N\boldsymbol{\Theta}. \quad (2.2)$$

Here N is the dimensionality of the parameter space; $N = 25$ for the pMSSM. Since the Bayesian evidence does not depend on the parameter values $\boldsymbol{\Theta}$, it is usually ignored in parameter estimation problems, and posterior inferences are obtained by exploring the unnormalized posterior using standard MCMC sampling methods. However, the evidence plays a central role in our discussion.

A useful feature of Bayesian parameter estimation is that one can easily obtain the posterior PDF of any function f of the model parameters $\boldsymbol{\Theta}$. Since

$$P(f|\mathbf{D}) = \int P(f, \boldsymbol{\Theta}|\mathbf{D})d\boldsymbol{\Theta} = \int P(f|\boldsymbol{\Theta}, \mathbf{D})P(\boldsymbol{\Theta}|\mathbf{D})d\boldsymbol{\Theta}$$
$$= \int \delta(f(\boldsymbol{\Theta}) - f)P(\boldsymbol{\Theta}|\mathbf{D})d\boldsymbol{\Theta}, \quad (2.3)$$

where the probability chain rule is employed for the second equality and δ is the Dirac delta function, one simply needs to compute $f(\boldsymbol{\Theta})$ for every Monte Carlo sample and the resulting sample will be drawn from $P(f|\mathbf{D})$. We make use of this feature in Secs. IV and V where we present the posterior probability PDFs of various observables used in the analysis of the pMSSM.

Before proceeding to discuss prior distributions, we first briefly address[2] the difference between the Bayesian and the frequentist approaches to inference. Bayesian inference (using Bayes' theorem) is a robust technique for updating prior knowledge or belief based on new data. It is unlike the frequentist approach where observations are viewed as random draws from some pool of possible observations such that the probability of an observation is the frequency observed with a large number of repeated measurements. Frequentists usually focus on the likelihood and argue that the Bayesian approach is too subjective because of the use of priors. Bayesians reply that when many examine frequentist statistics, they are actually implicitly using priors anyway. If one thinks of a region of parameter space with the lowest chi-squared values as being more likely than a region of parameter space with much higher chi-squared values, one is implicitly using some vague prior. The two approaches are asking different questions. Bayesians ask, "how likely is a given parameter value given the data?", while frequentists ask, "how probable are the data, given certain parameters?" In situations where the data are very informative, the two approaches give the same results. We are interested in PDFs of parameters and so we use Bayesian statistics. By comparing results from different but reasonable priors, we obtain an estimate of how robust an inference is given current data.

B. Priors

The prior probability of the model parameters is a PDF that gives a subjective measure of our initial knowledge or ignorance about the values of the parameters of the model before the data are taken. Symmetries and physical observations or expectations are usually a good guide to which priors to take. Information theory also provides a way of selecting priors by favoring those that maximize the entropy of the distributions. Some commonly used prior PDFs $P(\boldsymbol{\Theta}|H)$ are the following:

$$P(\boldsymbol{\Theta}|H) \propto \text{const} - \text{the linear prior, flat in } \boldsymbol{\Theta} \quad (2.4)$$

$$P(\boldsymbol{\Theta}|H) \propto \frac{1}{\boldsymbol{\Theta}} - \text{the Jeffreys prior, flat in } \log(\boldsymbol{\Theta}) \quad (2.5)$$

$$P(\boldsymbol{\Theta}|H) \propto e^{-(\boldsymbol{\Theta}-\bar{\boldsymbol{\Theta}})^2/2\sigma^2} - \text{the Gaussian prior.} \quad (2.6)$$

The linear priors are often used for translational (like time

[2]We follow the description in: http://www.dsg.port.ac.uk/valiviitaj/Lectures2006/CrittendenCMB2003.pdf

and location) parameters, where there is no information to suggest that one value is preferred over others. The Jeffreys prior, also referred to as logarithmic (log) prior, is uniform in the logarithm of the parameter. These two priors are improper since they diverge when integrated over an infinite range. Our log and linear priors will be bounded by the requirements of perturbativity of the model, by passing previous direct sparticle search constraints, and by the requirement of not too large fine-tuning in the Higgs potential parameters. These three criteria are sufficient to bound all 20 non-SM input parameters to a finite range. The Gaussian prior, on the other hand, is proper and integrable but requires previous experimental knowledge on σ and $\bar{\mathbf{\Theta}}$. This is indeed the case for our five SM input parameters, and we use Gaussian priors for them (see Sec. III A).

Assuming the parameters are independent, the resultant prior is obtained by the product of all the prior probability densities for each of the individual parameters. For instance, in the case of pMSSM with 25 parameters, $\theta_1, \theta_2, \ldots, \theta_{25}$,

$$P(\mathbf{\Theta}|H) \equiv \pi(\mathbf{\Theta}) = \prod_{i=1}^{25} \pi(\theta_i). \tag{2.7}$$

For our construction and analysis we are going to choose a linear prior measure for the pMSSM parameters described in Sec. III A. This is because there is no observational evidence that hints of giving preference to some parameter region over others. We are going to determine bounds on the parameters from the fact that the parameter values have to be not far away from the TeV scale in order to avoid the little hierarchy problem. We are going to call such case or scenario the *linear* prior. We then check the dependence of the results in our analysis of prior change by performing another analysis with a log prior. When we refer to a log prior, in fact, the Jeffreys prior is used only for all parameters that have only positive bounds. Parameters that are allowed to take either sign present a problem with Jeffreys priors since the prior diverges at the origin. Therefore, the priors of such parameters are always taken to be linear.

For parameter estimation, the priors become irrelevant once the data employed are powerful enough. This is already in evidence by comparing Bayesian CMSSM fits [34] with those in similar supersymmetric models that have a lower number of free parameters, for example, the large volume string compactification (LVS) scenario [23]. The LVS scenario has two less free parameters than the CMSSM, and current indirect data are already enough to make the result approximately prior independent. We may expect the addition of two precise, constraining, nondegenerate measurements (such as sparticle mass measurements from the LHC) to have the same effect upon the CMSSM.

For model comparison, the dependence on priors always remains (although with more informative data the degree of dependence on the priors is expected to decrease; see e.g. [27]). Indeed this explicit dependence on priors is one of the most attractive features of Bayesian model selection. References [13,35] identified prior distributions in high-scale CMSSM Lagrangian parameters. In particular, a Jacobian was defined to transform between derived parameters (such as $\tan\beta$) and more fundamental Lagrangian parameters from which they are derived. It is not our purpose here to find the ''most natural'' prior because any such choice is necessarily subjective. Instead, we shall check the robustness of any inference under a reasonable variation of the priors. Such a check is especially required in model comparison hypothesis tests, which may be particularly sensitive to the particular choice of prior and its associated metric in parameter space [36].

C. Model comparison

In order to evaluate and rank two alternative models H_0 and H_1 in the light of data $\mathbf{D}$, one needs to compare their respective posterior probabilities given the observed data set $\mathbf{D}$, as follows[3]: use Bayes' theorem to relate the plausibility of H_1 given the data, $P(H_1|\mathbf{D})$, to the predictions made by the model about the data, $P(\mathbf{D}|H_1)$, and the prior plausibility of H_1, $P(H_1)$. With this procedure one could construct the following probability ratio:

$$\frac{P(H_1|\mathbf{D})}{P(H_0|\mathbf{D})} = \frac{P(\mathbf{D}|H_1)P(H_1)}{P(\mathbf{D}|H_0)P(H_0)} = \frac{Z_1}{Z_0}\frac{P(H_1)}{P(H_0)}. \tag{2.8}$$

$P(H_1)/P(H_0)$ is the prior probability ratio for the two models, it measures how much our initial beliefs favor H_1 over H_2. It is often set to unity but may occasionally require further consideration. The other ratio, $P(\mathbf{D}|H_1)/P(\mathbf{D}|H_0)$, measures how well the observed data were predicted by H_1 and H_0. It can be seen from (2.8) that the Bayesian evidence takes the center stage in Bayesian model comparison. This technique was applied in [34] to compare two CMSSM models: $\mathrm{sign}(\mu) > 0$ versus $\mathrm{sign}(\mu) < 0$. We shall perform a similar comparison for the pMSSM in Sec. IV C. The comparison of different GUT scale SUSY-breaking models is also interesting [38].

The natural logarithm of the ratio of posterior model probabilities provides a useful guide to what constitutes a significant difference between two models:

$$\log\Delta E = \log\left[\frac{P(H_1|\mathbf{D})}{P(H_0|\mathbf{D})}\right] = \log\left[\frac{Z_1}{Z_0}\frac{P(H_1)}{P(H_0)}\right]. \tag{2.9}$$

In Table I we summarize the conventions we use in this paper to separate between different levels of evidence.

[3]Here we follow the description by [37].

TABLE I. The scale we use for the interpretation of model probabilities. Here the log represents the natural logarithm.

$\lvert\log\Delta E\rvert$	Odds, Z_1/Z_0	Probability	Remark
<1.0	$\lesssim 3{:}1$	<0.750	Inconclusive
1.0	$\sim 3{:}1$	0.750	Weak evidence
2.5	$\sim 12{:}1$	0.923	Moderate evidence
5.0	$\sim 150{:}1$	0.993	Strong evidence

III. THE PMSSM

The MSSM Lagrangian has the form $\mathcal{L} = \mathcal{L}_{\rm SUSY} + \mathcal{L}_{\rm soft}$ where $\mathcal{L}_{\rm SUSY}$ contains all of the kinetic terms, gauge, and Yukawa interactions while preserving SUSY invariance. It is based on the gauge group $G = SU(3)_c \times SU(2)_L \times U(1)_Y$ and superpotential W, constructed with a particle content in the following chiral superfields shown with their corresponding G charges:

$$\begin{aligned} &L\colon (1,2,-\tfrac{1}{2}), \quad \bar{E}\colon (1,1,1), \quad Q\colon (3,2,\tfrac{1}{6}),\\ &\bar{U}\colon (3,1,\tfrac{2}{3}), \quad \bar{D}\colon (3,1,-\tfrac{1}{3}), \quad H_1\colon (1,2,-\tfrac{1}{2}),\\ &H_2\colon (1,2,\tfrac{1}{2}). \end{aligned} \tag{3.1}$$

The superpotential is given by

$$\begin{aligned} W = \epsilon_{ab}[&(Y_E)_{ij} L_i^b H_1^a \bar{E}_j + (Y_D)_{ij} Q_i^{bx} H_1^a \bar{D}_{jx}\\ &+ (Y_U)_{ij} Q_i^{ax} H_2^b \bar{U}_{jx} + \mu H_2^a H_1^b]. \end{aligned} \tag{3.2}$$

Here we use the convention in [39] and denote the $SU(3)$ color index of the fundamental representation by $x, y = 1, 2, 3$; the $SU(2)_L$ fundamental representation indices by $a, b = 1, 2$; and the generation indices by $i, j = 1, 2, 3$. $\epsilon_{ab} = \epsilon^{ab}$ is the totally antisymmetric tensor, with $\epsilon_{12} = 1$.

The soft SUSY-breaking part of the Lagrangian consists of different mass and coupling terms:

$$\mathcal{L}_{\rm soft} = \mathcal{L}_{\rm gauginos} + \mathcal{L}_{\rm sfermions} + \mathcal{L}_{\rm trilinear} + \mathcal{L}_{\rm Higgs}, \tag{3.3}$$

where the part including the SUSY-breaking sfermion masses is

$$\begin{aligned} -\mathcal{L}_{\rm sfermion} = &\tilde{Q}^*_{ixa} (m^2_{\tilde{Q}})_{ij} \tilde{Q}^{xa}_j + \tilde{L}^*_{ia} (m^2_{\tilde{L}})_{ij} \tilde{L}^a_j\\ &+ \tilde{u}^x_i (m^2_{\tilde{u}})_{ij} \tilde{u}^*_{jx} + \tilde{d}^x_i (m^2_{\tilde{d}})_{ij} \tilde{d}^*_{jx} + \tilde{e}_i (m^2_{\tilde{e}})_{ij} \tilde{e}^*_j. \end{aligned} \tag{3.4}$$

Each mass parameter in Eq. (3.4) is a 3×3 Hermitian matrix in generation space.

$$\begin{aligned} -\mathcal{L}_{\rm Higgs} = &m^2_{H_1} H^*_{1a} H^a_1 + m^2_{H_2} H^*_{2a} H^a_2\\ &+ \epsilon_{ab} (m^2_3 H^a_2 H^b_1 + \text{H.c.}) \end{aligned} \tag{3.5}$$

gives the SUSY-breaking Higgs masses and bilinear coupling terms. The SUSY-breaking scalar trilinear couplings are

$$\begin{aligned} -\mathcal{L}_{\rm trilinear} = \epsilon_{ab}[&\tilde{Q}^{xa}_{i_L} (U_A)_{ij} \tilde{u}^*_{jx_R} H^b_2 + \tilde{Q}^{xb}_{i_L} (D_A)_{ij} \tilde{d}^*_{jx_R} H^a_1\\ &+ \tilde{L}^b_{i_L} (E_A)_{ij} \tilde{e}^*_{j_R} H^a_1] + \text{H.c.}, \end{aligned} \tag{3.6}$$

where fields with a tilde represent the scalar components of the corresponding capital letter superfield and the soft SUSY-breaking A terms, each a complex 3×3 matrix in generation space, are defined (no summation on i, j is inferred) as

$$(A_{U,D,E})_{ij} = (U_A, D_A, E_A)_{ij} / (Y_{U,D,E})_{ij}. \tag{3.7}$$

Finally, writing the bino as $\tilde{b}$, $\tilde{w}^{A=1,2,3}$ as the unbroken-$SU(2)_L$ gauginos and $\tilde{g}^{X=1,\ldots,8}$ as the gluinos, then the gaugino-mass part of the Lagrangian is

$$\begin{aligned} -\mathcal{L}_{\rm gaugino} = \frac{1}{2}\Big[&M_1 \tilde{b}\,\tilde{b} + M_2 \sum_{A=1}^{3} \tilde{w}^A \tilde{w}^A\\ &+ M_3 \sum_{X=1}^{8} \tilde{g}^X \tilde{g}^X + \text{H.c.} \Big]. \end{aligned} \tag{3.8}$$

The parameters together make a total of 105 free parameters in $\mathcal{L}_{\rm soft}$, before rephasing and Higgs potential minimization [24,40,41]. In the CMSSM, the SUSY-breaking scalar masses, the gaugino masses, and trilinear couplings are collapsed to the flavor independent parameters m_0, $M_{1/2}$, and A_0, respectively, at grand unification scales $M_{\rm GUT} \sim 2 \times 10^{16}$ GeV. m_3^2 and $|\mu|$ are related to the Z-boson mass m_Z through Higgs potential minimization conditions. $\text{sign}(\mu) = \pm$ and $\tan\beta$, the ratio of the Higgs vacuum expectation values (vevs), remain as free parameters. However, in this paper we instead explore the parameters at the weak scale in its phenomenologically most relevant directions and following Ref. [42] call the setup the pMSSM. In Sec. III A we describe how the 25 parameters in the pMSSM setup are derived from the much larger parameter space of the parent MSSM.

A. Parameters

Sources of CP violation in the MSSM are tightly constrained by experimental limits on the electron and neutron electric dipole moments and from results on the K-meson system experiments. Assuming that the MSSM soft SUSY-breaking parameters are real is consistent with such tight bounds; indeed significant departures from this assumption usually require a specific cancellation or suppression mechanism in order to pass the constraints. To suppress flavor changing neutral current processes, all off-diagonal elements in the sfermions masses and trilinear couplings are set to zero and the first and second generation soft terms are set to be equal. A_t, A_b, and A_τ may all change the likelihood significantly, and we also include $A_e = A_\mu$ because it is relevant for the computation of the anomalous magnetic moment of the muon [43]. We set $A_u = A_c = A_d = A_s = 0$ since these are proportional to the SM Yukawa couplings, which are very tiny, and so they will

have negligible effect on the likelihood. All the other trilinear couplings are set to zero. Our Higgs-sector parameters are specified by $(m^2_{H_1}, m^2_{H_2})$, and as discussed above, we must add $\tan\beta$ and $\mathrm{sign}(\mu)$ to the list of parameters.

All of the parameters mentioned so far are purely non-SM. However, some of the SM parameters significantly affect the likelihood. The relevant SM parameters include the electromagnetic coupling constant $\alpha_{\mathrm{em}}(m_Z)^{\overline{\mathrm{MS}}}$ and the strong coupling constant $\alpha_s(m_Z)^{\overline{\mathrm{MS}}}$. The values of these two couplings are taken at the Z-boson pole mass m_Z energy scale evaluated in the $\overline{\mathrm{MS}}$ renormalization scheme. The tau lepton mass and G_F, the Fermi constant, have been so precisely determined that their uncertainty has negligible error on the likelihood, and so they are fixed at their global average values: $m_\tau = 1.777$ GeV and $G_F = 1.166\,37 \times 10^{-5}$ GeV^{-2} [44]. The top and bottom quark masses are not as precisely known and can have significant effects on predictions of supersymmetric models. They are therefore included as parameters with, using the experimental measurements of their central values and uncertainties, Gaussian priors. Despite the fact that the Z-boson mass, m_Z, is precisely determined, we include its uncertainty because one of the observables used for the analysis (the total decay width of the Z-boson Γ_Z) is proportional to m_Z^3 and the pMSSM predicted values can fall outside the expected experimentally determined range with a sigma variation in m_Z. So adding the SM parameters,

$$\theta_{\mathrm{SM}} = \{m_Z, m_t, m_b(m_b)^{\overline{\mathrm{MS}}}, \alpha_{\mathrm{em}}(m_Z)^{\overline{\mathrm{MS}}}, \alpha_s(m_Z)^{\overline{\mathrm{MS}}}\}, \tag{3.9}$$

makes a total of 25 continuously varying parameters in the pMSSM. These are listed together with their ranges or Gaussian prior distributions in Table II. These pMSSM directions make up its parameter space. Our aim is to eventually construct a detailed map of the parameter space that could be a help to or a guide for collider and other SUSY-related experiments. In Sec. III B we briefly describe the observables considered and summarize the experimental constraints coming from each.

B. Observables and experimental constraints

The SM fits high precision electroweak data well [46]. However, on the one hand, there are some observables whose SM predicted values significantly differ from the corresponding experimental indications. The discrepancies could be explained by the direct or indirect presence of supersymmetric particles (or sparticles) in the interactions. On the other hand, the very precise agreement between the

TABLE II. The 25 parameters of the pMSSM model. The first 20 non-SM parameters are listed with their corresponding prior range. Gaussian priors are used for the SM parameters, which are the last five listed, along with their central values and standard deviations.

Parameter	Description	Prior range
M_1	Bino mass	$[-4$ TeV, 4 TeV$]$
M_2	Wino mass	$[-4$ TeV, 4 TeV$]$
M_3	Gluino mass	$[-4$ TeV, 4 TeV$]$
$m_{\tilde{e}_L} = m_{\tilde{\mu}_L}$	1st/2nd generation L_L slepton	[100 GeV, 4 TeV]
$m_{\tilde{\tau}_L}$	3rd generation L_L slepton	[100 GeV, 4 TeV]
$m_{\tilde{e}_R} = m_{\tilde{\mu}_R}$	1st/2nd generation E_R slepton	[100 GeV, 4 TeV]
$m_{\tilde{\tau}_R}$	3rd generation E_R slepton	[100 GeV, 4 TeV]
$m_{\tilde{u}_L} = m_{\tilde{d}_L} = m_{\tilde{c}_L} = m_{\tilde{s}_L}$	1st/2nd generation Q_L squark	[100 GeV, 4 TeV]
$m_{\tilde{t}_L} = m_{\tilde{b}_L}$	3rd generation Q_L squark	[100 GeV, 4 TeV]
$m_{\tilde{u}_R} = m_{\tilde{c}_R}$	1st/2nd generation U_R squark	[100 GeV, 4 TeV]
$m_{\tilde{t}_R}$	3rd generation U_R squark	[100 GeV, 4 TeV]
$m_{\tilde{d}_R} = m_{\tilde{s}_R}$	1st/2nd generation D_R squark	[100 GeV, 4 TeV]
$m_{\tilde{b}_R}$	3rd generation D_R squark	[100 GeV, 4 TeV]
A_t	Trilinear coupling for top quark	$[-8$ TeV, 8 TeV$]$
A_b	Trilinear coupling for b quark	$[-8$ TeV, 8 TeV$]$
A_τ	Trilinear coupling for τ quark	$[-8$ TeV, 8 TeV$]$
$A_e = A_\mu$	Trilinear coupling for μ quark	$[-8$ TeV, 8 TeV$]$
m_{H_1}	Up-type Higgs doublet mass	$[-4$ TeV, 4 TeV$]$
m_{H_2}	Down-type Higgs doublet mass	$[-4$ TeV, 4 TeV$]$
$\tan\beta$	Scalar doublets vevs ratio	[2, 60]
m_t	Top quark mass [45]	172.6 ± 1.4
m_Z	Z-boson mass	91.187 ± 0.021
$m_b(m_b)^{\overline{\mathrm{MS}}}$	b-quark mass	4.20 ± 0.07
$1/\alpha_{\mathrm{em}}(m_Z)^{\overline{\mathrm{MS}}}$ [44]	Electromagnetic coupling constant	127.918 ± 0.018
$\alpha_s(m_Z)^{\overline{\mathrm{MS}}}$	Strong coupling constant	0.117 ± 0.002

SM prediction and the experimentally determined values of some other set of observables could be altered by the presence of non-SM particles. The absence of any significant such deviation puts tight constraints on possible new physics beyond the SM (SUSY in our case); see, for instance, [47,48], and references therein. The values of the sparticle masses affect these tendencies. For instance, the effect of sparticles in loop corrections to electroweak physics observables (EWPO) decouple if their masses are much heavier than m_Z (300 GeV and above according to Ref. [49]). Lighter sparticles with masses just above current experimental limits will contribute to the discrepancy between some experimentally determined electroweak quantities and their corresponding SM predictions—hence the preference for low-energy (weak-scale) SUSY in accounting for such differences.

For the pMSSM setup we use observables and constraints from high precision collider measurements that are sensitive to effects of new physics via virtual loops. These include five EWPO: the W-boson mass, m_W, the effective leptonic weak mixing angle, $\sin^2\theta^{\rm lep}_{\rm eff}$, the total Z-boson decay width, Γ_Z, the anomalous magnetic moment of the muon, $(g-2)_\mu$, and the mass of the lightest MSSM Higgs boson, m_h; five B-physics observables: branching ratios $\mathrm{BR}(B \to X_s\gamma)$, $\mathrm{BR}(B_s \to \mu^+\mu^-)$, $\mathrm{BR}(B_{u^-} \to \tau^-\nu)$, $\mathrm{BR}(B_u \to K^*\gamma)$, and the B_s mass-mixing parameter ΔM_{B_s}; and the cosmological observable, dark matter relic density from WMAP5 results. We next briefly describe each of these physical observables and state the corresponding experimental constraints. We first discuss constraints from EWPO and end the section with discussion of sparticle mass limits.

(i) *W-boson mass, m_W*: The CDF Run II electroweak public results cited the W-boson mass measurement as the single most precise measurement to date and quotes [50]

$$m_W = (80.399 \pm 0.025)\ \mathrm{GeV}. \tag{3.10}$$

Theoretically the mass can be calculated from

$$m_W = \frac{\pi\alpha_{\rm em}}{\sqrt{2}G_F(1 - m_W^2/m_Z^2)(1-\Delta r)}, \tag{3.11}$$

where $\alpha_{\rm em}$ is the fine structure constant at the m_Z renormalization energy scale, G_F is the Fermi weak coupling constant, and Δr includes all radiative corrections to the mass (see e.g. [51,52], and references therein). The high precision in this measured quantity constrains any radiative corrections from new physics effects. The experimental precision is very high to the extent that measurements can be sensitive even to two-loop effects involving sparticles. We include a theoretical uncertainty of 10 MeV on m_W by adding it in quadrature with the experimental uncertainty. We use SUSYPOPE [53,54] to calculate the W-boson mass m_W and the other EWPO. The most complete available SM two-loop corrections and the dominant results for two-loop SUSY corrections as implemented in SUSYPOPE currently give the most accurate predictions within the MSSM.

(ii) *Z-boson decay width, Γ_Z*: The partial Z-boson decay width in the massless fermion limit ($m_f^2/m_Z^2 \to 0$) is given by [55]

$$\Gamma_{Z\to f\bar f} = N_c^f \frac{G_F m_Z^3}{6\sqrt{2}\pi}\delta_{\rm QCD}(\bar g_v^{(f)2} + \bar g_a^{(f)2}) + \Delta_{\rm ew/QCD}, \tag{3.12}$$

where $\bar g_{v,a}$ are the neutral weak coupling constants modified to include electroweak (EW) radiative effects, $\delta_{\rm QCD}$ parameterizes the QCD corrections, and $\Delta_{\rm ew/QCD}$ includes some nonfactorizable EW contributions. The color factor N_c^f is 1 for leptons and 3 for quarks. The current experimental value for the total decay width is [50]

$$\Gamma_Z = (2.4952 \pm 0.0023)\ \mathrm{GeV}. \tag{3.13}$$

Theoretically

$$\Gamma_Z = \Gamma_l + \Gamma_h + \Gamma_{\rm inv}, \tag{3.14}$$

where $\Gamma_{l,h}$ are the decay widths into SM leptons and quarks. $\Gamma_{\rm inv}$ is for the decays into invisible particles (neutrinos and possibly, if they are light enough, neutralinos). Supersymmetric contributions enter via virtual corrections to the partial decay widths into leptons and quarks.

(iii) *Effective mixing angle, $\sin^2\theta^{\rm lep}_{\rm eff}$*: The effective electroweak mixing angle depends only on the ratio of the effective weak couplings

$$\mathrm{Re}\,(g_v/g_a) = 1 - 4\sin^2\theta^{\rm lep}_{\rm eff} \tag{3.15}$$

for the vertex that couples the Z boson and leptons l in the Lagrangian: $i\bar l\gamma^\mu(g_v - g_a\gamma_5)Z_\mu l$. It is determined from various asymmetry measurements around the Z-boson peak from e^+e^- colliders after removing QED effects [56]. We use the experimental estimate corresponding to the flavor inclusive forward-backward asymmetry [50]

$$\sin^2\theta^{\rm lep}_{\rm eff} = 0.2324 \pm 0.0012. \tag{3.16}$$

(iv) *Z-pole asymmetry parameters from $e^+e^- \to f\bar f$ processes*: The results from the LEP and SLC e^+e^- colliders on Z-boson properties (its mass, partial and total widths, and couplings to fermion pairs) are in good agreement with the SM predictions [56]. The precision is high enough to probe loop-level predictions where both SM and beyond the SM corrections are absorbed into effective coupling constants. The LEP data consist of hadronic

and leptonic cross sections, leptonic forward-backward asymmetries, τ polarization asymmetries, $b\bar{b}$ and $c\bar{c}$ partial widths, and forward-backward asymmetries. The Z-boson parameters derived from the data that we employ for our analysis include the ratios R_l (which we assume to be the average of R_e, R_μ, and R_τ), R_b, and R_c. These are defined as

$$R_b = \frac{\Gamma(Z \to b\bar{b})}{\Gamma(Z \to \text{hadrons})},$$
$$R_c = \frac{\Gamma(Z \to c\bar{c})}{\Gamma(Z \to \text{hadrons})}, \qquad (3.17)$$
$$R_l = \frac{\Gamma(Z \to l^+ l^-)}{\Gamma(Z \to \text{hadrons})}$$

and are constrained to be

$$R_b = 0.216\,29 \pm 0.000\,66,$$
$$R_c = 0.1721 \pm 0.0030, \quad \text{and}$$
$$R_l = 20.767 \pm 0.025.$$

The Z boson interacts with fermions through a mixture of vector and axial-vector couplings. This makes the strength of the interaction between left- and right-handed fermions unequal and leads to the production of polarized Z bosons at the e^+e^- colliders. As a result, there are measurable asymmetries (such as a forward-backward asymmetry) in the angular distributions of the final-state fermions $f\bar{f}$. The forward-backward asymmetry is related to the probability that the $\bar{f}$ travels in the same (forward) or opposite (backward) direction to the incident e^- direction and is quantified by

$$A_{FB} = \frac{\sigma_F - \sigma_B}{\sigma_F + \sigma_B}, \qquad (3.18)$$

where σ_F (σ_B) is the cross section in the forward (backward) directions. In terms of the effective vector and axial-vector neutral current couplings, g_{Vf} and g_{Af}, respectively, other Z-pole asymmetries are

$$A_{FB}^{0,f} = \frac{3}{4}\mathcal{A}^e\mathcal{A}^f, \qquad \mathcal{A}^f \equiv \frac{2g_{Vf}g_{Af}}{g_{Vf}^2 + g_{Af}^2}. \qquad (3.19)$$

Here A^f gives a measure of the asymmetry for the different possible final-state fermions. At LEP the Z-pole forward-backward asymmetries $A_{FB}^{0,b}$ and $A_{FB}^{0,c}$ were precisely measured for the final states $b\bar{b}$ and $c\bar{c}$, respectively. We impose $A_{FB}^{0,b} = 0.0992 \pm 0.0016$ and $A_{FB}^{0,c} = 0.0707 \pm 0.0035$ for our analysis.

Using polarized beams, the Stanford Large Detector experiment made a direct and precise measurement of the parameter A_e from the left-right asymmetry

$$A_{LR} = \frac{\sigma_L - \sigma_R}{\sigma_L + \sigma_R}, \qquad (3.20)$$

where σ_L and σ_R are the e^+ e^- production cross sections for Z bosons produced with left- and right-handed electrons, respectively. The same parameter, A^e, is also indirectly constrained by LEP experiments. Using the measurements of A^e, the parameters A^μ, A^τ, A^b, and A^c can then be inferred from A_{FB} measurements at LEP. Hence, the LEP and SLC results form a complete set of the A^f parameter measurements. The asymmetry parameter constraints we use are $A^b = 0.923 \pm 0.020$, $A^c = 0.670 \pm 0.027$, and $A^l = 0.1513 \pm 0.0021 = A^e$.

(v) *Muon anomalous magnetic moment*, δa_μ: The world average for the muon anomalous magnetic moment as determined from $e^+e^- \to$ hadrons-based experiment at Brookhaven [57] is $a_\mu^{\text{exp}} \equiv \frac{1}{2}(g-2)_\mu = 1\,165\,920.80 \pm 0.63 \times 10^{-9}$. Other results from experiments based on the τ lepton decay to hadrons [58–60] differ slightly, and we are not using those here.[4] The experimental results are around 3σ deviation from the SM prediction [62] $a_\mu^{\text{SM}} = 1\,165\,917.85 \pm 0.61 \times 10^{-9}$ giving

$$\delta a_\mu = a_\mu^{\text{exp}} - a_\mu^{\text{SM}} = 29.5 \pm 8.8 \times 10^{-10}. \qquad (3.21)$$

SUSY is a good new physics candidate that can explain this deviation. For sparticles all of mass M_{SUSY}, their contribution to a_μ is of order [63]

$$a_\mu^{\text{SUSY}} \approx 13 \times 10^{-10}\left(\frac{100\ \text{GeV}}{M_{\text{SUSY}}}\right)\tan\beta\ \text{sign}(\mu). \qquad (3.22)$$

We use `micrOMEGAs` [64–67] to predict a_μ, correcting it with Δ_μ, which includes contributions from the dominant QED-logarithmic piece, some dominant two-loop corrections [61], and the recently computed $\tan\beta$-enhanced term (see [68], and references therein)

$$a_\mu^{\text{SUSY}} = a_\mu^{\text{SUSY,1L}}\left(1 - \frac{4\alpha}{\pi}\log\frac{M_{\text{SUSY}}}{m_\mu}\right)\left(\frac{1}{1+\Delta_\mu}\right) + \text{2-loop terms}. \qquad (3.23)$$

For our analysis we add in quadrature a theoretical

[4] See [61] for a recent review.

error of 2.0×10^{-10} to the 8.8×10^{-10} error above and use the average value $\delta a_\mu = (30.2 \pm 9.2) \times 10^{-10}$.

δa_μ is somewhat smaller if one uses it from τ lepton decay rather than e^+e^- experiments to infer the hadronic contributions [69]. With τ data, there is still a 1.9σ discrepancy between the SM prediction and the measured value of $(g-2)_\mu$. We expect the sparticles involved (particularly the smuons, light charginos, and neutralinos) to therefore be slightly heavier on average if one used the τ data instead. However, we do not expect a large change if we instead used the τ data to extract a_μ.

(vi) *Lightest Higgs boson mass*, m_h: The SM Higgs mass is constrained to $m_h \geq 114.4$ GeV by LEP direct search experiment (see e.g. [70], and references therein). The predicted Higgs mass can be parametrized by $g_{hZZ}/g_{hZZ}^{\rm SM}$, the ratio of the MSSM Higgs coupling to two neutral Z bosons to the equivalent SM coupling. In the MSSM $g_{hZZ}/g_{hZZ}^{\rm SM} = \sin^2(\beta-\alpha)$, so we use the above LEP mass limit for $\sin^2(\beta-\alpha) > 0.95$ and use the MSSM Higgs mass limit $m_h \geq 89.7$ for $\sin^2(\beta-\alpha) < 0.95$.

(vii) *Branching ratio* $(B \to X_s\gamma)$: The experimental value of the decay rate of the flavor changing process $B \to X_s\gamma$ agrees to high precision with the SM prediction. This stringently constrains new physics models that may contribute to the process. For SUSY the leading contributions come from loops with charged Higgs bosons (these interfere constructively with the SM contributions) and charginos. Loops with neutralinos are small (see, for instance, [71]). A recent theoretical estimate for the SM contribution to the branching ratio of $B \to X_s\gamma$, which we call $\mathrm{BR}(b \to s\gamma)$ at next-to-next-to leading order (NNLO) in QCD, is $\mathrm{BR}(b \to s\gamma)_{\rm SM} = (3.28 \pm 0.23) \times 10^{-4}$ [72–75], where a 1.6 GeV lower energy cut is applied to the photon. The central value is $\sim 1\sigma$ lower than a world-average experimental value from the Heavy Flavor Averaging Group (HFAG) [76][5]:

$$\mathrm{BR}(B \to X_s\gamma)_{\rm exp} = (3.55 \pm 0.22^{+0.09}_{-0.10} \pm 0.03) \times 10^{-4}. \quad (3.24)$$

The values predicted for this observable at different parameter points are constrained by combining in quadrature the experimental and SM prediction errors:

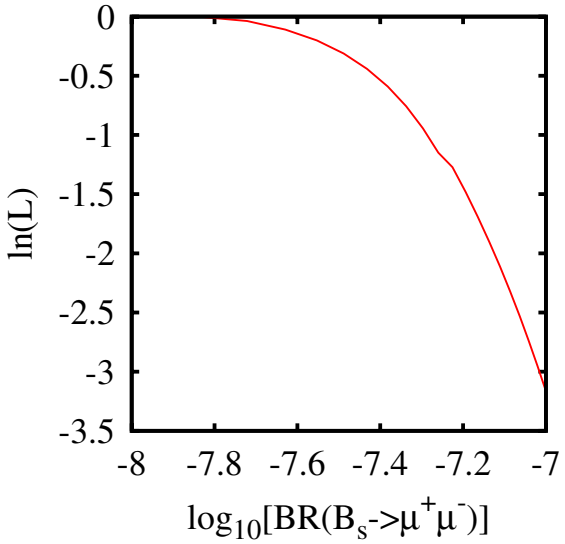

FIG. 1 (color online). Likelihood penalty on the predicted value of $\mathrm{BR}(B_s \to \mu^+\mu^-)$.

$$\mathrm{BR}\,(B \to X_s\gamma)_{\rm exp} = (3.55 \pm 0.42) \times 10^{-4}. \quad (3.25)$$

The branching ratio therefore constrains non-SM contributions. We use SUPERISO2.0 [77] to predict the MSSM plus SM branching ratio.[6]

(viii) *Branching ratio* $(B_s \to \mu^+\mu^-)$: The branching fraction for the flavor changing process $B_s \to \mu^+\mu^-$ is predicted to be $(3.42 \pm 0.54) \times 10^{-9}$ within the SM [79]. In the MSSM, interactions involving neutral Higgs bosons can enhance the branching fraction by several orders of magnitude at high $\tan\beta$. The branching ratio is experimentally bounded from above by recent CDF II results, implying

$$\mathrm{BR}\,(B_s \to \mu^+\mu^-) < 5.8 \times 10^{-8} \quad (3.26)$$

at 95% C.L. [80]. We apply a continuous likelihood constraint derived from CDF II data upon the MSSM prediction [81]. The resulting penalty is shown in Fig. 1.

(ix) B_s-$\bar{B}_s$ *mass difference*, ΔM_{B_s}: The neutral B-meson oscillates between particle and antiparticle states via flavor changing processes. The frequency of oscillation is proportional to the mass difference ΔM_{B_s}. It has been measured to be $(\Delta M_{B_s})_{\rm exp} = 17.77 \pm 0.12\ \mathrm{ps}^{-1}$ [82]. Its SM prediction can be obtained from an overall unitarity triangle fit: $(\Delta M_{B_s})_{\rm SM} = 20.9 \pm 2.6\ \mathrm{ps}^{-1}$ [83]. We use the ra-

[5]We note that the most recent central value has shifted slightly to 3.52: this small change would leave no significant imprint on our fits.

[6]The program `SusyBSG` [78] now contains a more accurate prediction of this branching ratio to two loops in MSSM parameters. It could lead to an estimated shift in the predicted branching ratio of 0.13×10^{-4}, which may be considered to be included within our estimate of theoretical error.

tio of the experimental constraint to the SM prediction,

$$R^{\rm exp}_{\Delta M_{B_s}} = \frac{(\Delta M_{B_s})_{\rm exp}}{(\Delta M_{B_s})_{\rm SM}} = 0.85 \pm 0.11, \qquad (3.27)$$

to constrain the predicted frequencies. Our pMSSM predicted values are based on the results in [84], and references therein:

$$\begin{aligned} R^{\rm MSSM}_{\Delta M_{B_s}} &= \frac{(\Delta M_{B_s})_{\rm MSSM}}{(\Delta M_{B_s})_{\rm SM}} \\ &= 1 - \frac{64\pi \sin^2\theta_w}{\alpha_{\rm em} M_A^2 S_0(m_t^2/m_W^2)} \\ &\quad \times \frac{m_b(\mu_b) m_s(\mu_b)(\epsilon_Y \tan^2\beta)^2}{[1 + (\epsilon_0 + \epsilon_Y)\tan\beta]^2 [1 + \epsilon_0 \tan\beta]^2}, \end{aligned} \qquad (3.28)$$

where $m_{b,s}$ are the bottom- and strange-quark masses evaluated at the $\overline{\rm MS}$ scale $\mu_b = m_b$;

$$\begin{aligned} \epsilon_0 &= -\frac{2\alpha_s \mu}{3\pi m_{\tilde g}} H_2\left(\frac{m^2_{\tilde q L}}{m^2_{\tilde g}}, \frac{m^2_{dR}}{m^2_{\tilde g}}\right), \\ \epsilon_Y &= -\frac{A_t y_t^2}{16\pi^2 \mu} H_2\left(\frac{m^2_{\tilde q L}}{\mu^2}, \frac{m^2_{\tilde u R}}{\mu^2}\right) \end{aligned} \qquad (3.29)$$

are the effective couplings that parameterize the correction to the down-type Yukawa couplings,

$$H_2(x, y) = \frac{x \log x}{(1-x)(x-y)} + \frac{y \log y}{(1-y)(y-x)}; \qquad (3.30)$$

μ is the supersymmetric Higgs mass terms and A_t is the trilinear soft-breaking term involving the stops. S_0 is given by

$$S_0(x) = \frac{4x - 11x^2 + x^3}{4(1-x)^2} - \frac{3x^3 \log x}{2(1-x)^3}.$$

(x) *Branching ratio* ($B_u \to \tau\nu$): The purely leptonic decay $B_{u^-} \to \tau^- \nu$ proceeds via the annihilation of b and $\bar u$ quarks into W^-. The SM prediction for the branching ratio of the process is given by

$$\mathrm{BR}(B_u \to \tau\nu)_{\rm SM} = \frac{G_F^2 m_B m_\tau^2}{8\pi}\left[1 - \frac{m_\tau^2}{m_B^2}\right]^2 f_B^2 |V_{ub}|^2 \tau_B, \qquad (3.31)$$

where m_B and m_τ are the B meson and τ pole masses, respectively, and τ_B is the B^--meson lifetime. For the SM prediction we use the average of the result from unitarity triangle fits [$\mathrm{BR}(B_u \to \tau\nu) = 0.85 \pm 0.14 \times 10^{-4}$] and the result obtained from the experimental determination of V_{ub} and $f_B\sqrt{B_{B_d}}$ [$\mathrm{BR}(B_u \to \tau\nu) = 1.39 \pm 0.44 \times 10^{-4}$][7] adding the errors in quadrature to

$$\mathrm{BR}\,(B_u \to \tau\nu)_{\rm SM} = 1.12 \pm 0.46 \times 10^{-4}. \qquad (3.32)$$

For the experimental constraint upon the branching ratio, we use the average of the Belle and *BABAR* experiments, adding their errors in quadrature:

$$\mathrm{BR}\,(B_u \to \tau\nu)_{\rm exp} = 1.41 \pm 0.43 \times 10^{-4}. \qquad (3.33)$$

Equations (3.32) and (3.33) are then used to form the constraint

$$R^{\rm exp}_{B\tau\nu} = \frac{\mathrm{BR}(B_u \to \tau\nu)_{\rm exp}}{\mathrm{BR}(B_u \to \tau\nu)_{\rm SM}} = 1.26 \pm 0.41. \qquad (3.34)$$

For the pMSSM predictions we follow [48] and predict

$$\begin{aligned} R^{\rm MSSM}_{B\tau\nu} &= \frac{\mathrm{BR}(B_u \to \tau\nu)_{\rm MSSM}}{\mathrm{BR}(B_u \to \tau\nu)_{\rm SM}} \\ &= \left[1 - \left(\frac{m^2_{B_u}}{m^2_{H^\pm}}\right)\frac{\tan^2\beta}{1 + \epsilon_0 \tan\beta}\right]^2, \end{aligned} \qquad (3.35)$$

where ϵ_0 is the effective coupling defined in Eq. (3.29), m_{B_u} is the B-meson mass, and $m_{H^\pm}$ is the charged Higgs boson mass.

(xi) Δ_{0-}: $B \to K^*\gamma$ *Isospin asymmetry*: Isospin symmetry predicts the amplitudes for the decays $\bar B^0 \to \bar K^{*0}\gamma$ and $B^- \to K^{*-}\gamma$ to be equal at leading order in perturbation theory. Isospin-breaking effects in the process $B \to K^*\gamma$ [85] may therefore provide a sensitive probe of physics beyond the SM. The isospin asymmetry for the exclusive process $B \to K^*\gamma$ is defined as

$$\Delta_{0-} = \frac{\Gamma(\bar B^0 \to \bar K^{*0}\gamma) - \Gamma(B^- \to K^{*-}\gamma)}{\Gamma(\bar B^0 \to \bar K^{*0}\gamma) + \Gamma(B^- \to K^{*-}\gamma)}. \qquad (3.36)$$

The world-average experimental value is [44]

$$\Delta_{0-} = 0.0375 \pm 0.0289. \qquad (3.37)$$

In order to fit this, we use the MSSM prediction from `SuperIso2.0` [77], which contains the available next-to-leading-order (NLO) contributions to Δ_{0-}, including the complete supersymmetric QCD corrections to Wilson coefficient operators. It also includes some partial NNLO SM QCD corrections.

(xii) *Dark matter relic density*: The Wilkinson Microwave Anisotropy Probe (WMAP) fits to a cosmological constant plus cold dark matter model

[7] See "New Constraints from B and K Rare Decays" at http://www.utfit.org/.

TABLE III. Summary of constraints on predictions. Theoretical uncertainties have been added in quadrature to the experimental uncertainties quoted.

Observable	Constraint	Th. source	Ex. source
m_W [GeV]	80.399 ± 0.027	[54]	[87]
Γ_Z [GeV]	2.4952 ± 0.0025	[53]	[56]
$\sin^2\theta^{\rm lep}_{\rm eff}$	0.2324 ± 0.0012	[54]	[56]
δa_μ	$(30.2 \pm 9.0) \times 10^{-10}$	[88–91]	[57,58,60]
R^0_l	20.767 ± 0.025	[53]	[56]
R^0_b	$0.216\,29 \pm 0.000\,66$	[53]	[56]
R^0_c	0.1721 ± 0.0030	[53]	[56]
$A^b_{\rm FB}$	0.0992 ± 0.0016	[53]	[56]
$A^c_{\rm FB}$	0.0707 ± 0.035	[53]	[56]
$A^l = A^e$	0.1513 ± 0.0021	[53]	[56]
A^b	0.923 ± 0.020	[53]	[56]
A^c	0.670 ± 0.027	[53]	[56]
$\mathrm{Br}(B \to X_s\gamma)$	$(3.55 \pm 0.42) \times 10^{-4}$	[72–74,92]	[76]
$\mathrm{Br}(B_s \to \mu^+\mu^-)$	see Fig. 1	[64–67]	[80]
$R_{\Delta M_{B_s}}$	0.85 ± 0.11	[83]	[82]
$R_{\mathrm{Br}(B_u\to\tau\nu)}$	1.26 ± 0.41	[84,93,94]	[95–97]
Δ_{0-}	0.0375 ± 0.0289	[77]	[44]
$\Omega_{\rm CDM}h^2$	0.11 ± 0.02	[64–67]	[86]

TABLE IV. The lower bounds applied to MSSM particle masses.

Condition	Sparticle mass	Lower bound/GeV
$\sin^2(\alpha-\beta) > 0.95$	m_h	114
$\sin^2(\alpha-\beta) \le 0.95$	m_h	89.7
$m_{\tilde\tau_1} - m_{\tilde\chi^0_1} > 10$ GeV	$m_{\tilde\tau_1}$	87
$m_{\tilde\tau_1} - m_{\tilde\chi^0_1} \le 10$ GeV	$m_{\tilde\tau_1}$	73
$m_{\tilde e_R} - m_{\tilde\chi^0_1} > 10$ GeV	$m_{\tilde e_R}$	100
$m_{\tilde e_R} - m_{\tilde\chi^0_1} \le 10$ GeV	$m_{\tilde e_R}$	73
$m_{\tilde\mu_R} - m_{\tilde\chi^0_1} > 10$ GeV	$m_{\tilde\mu_R}$	95
$m_{\tilde\mu_R} - m_{\tilde\chi^0_1} \le 10$ GeV	$m_{\tilde\mu_R}$	73
$m_{\tilde\nu_e} - m_{\tilde\chi^0_1} > 10$ GeV	$m_{\tilde\nu_e}$	94
$m_{\tilde\nu_e} - m_{\tilde\chi^0_1} \le 10$ GeV	$m_{\tilde\nu_e}$	43
$m_{\tilde\nu_\tau} > 300$ GeV	$m_{\tilde\chi^\pm_1}$	43
$m_{\tilde\nu_\tau} \le 300$ GeV	$m_{\tilde\chi^\pm_1}$	92.4
$\cdots$	$m_{\tilde\chi^0_1}$	50
$m_{\tilde t} - m_{\tilde\chi^0_1} > 10$ GeV	$m_{\tilde t}$	95
$m_{\tilde t} - m_{\tilde\chi^0_1} \le 10$ GeV	$m_{\tilde t}$	65
$m_{\tilde t} - m_{\tilde\chi^0_1} > 10$ GeV	$m_{\tilde b}$	95
$m_{\tilde t} - m_{\tilde\chi^0_1} \le 10$ GeV	$m_{\tilde b}$	59
$\cdots$	$m_{\tilde q}$	318
$\cdots$	$m_{\tilde g}$	195

(ΛCDM) imply a dark matter relic density of $\Omega_{\rm DM}h^2 = 0.1143 \pm 0.0034$, where h is the reduced Hubble constant [86]. We assume R parity, resulting in a stable lightest supersymmetric particle (LSP). The neutralino, $\tilde\chi^0_1$, LSP then has the correct properties to make up the cold dark matter, being massive, stable, and neutral, and we constrain the prediction of its relic density to lie on the WMAP5 central value, but inflate the uncertainties with an assumed error on the theoretical prediction:

$$\Omega_{\rm DM}h^2 = 0.1143 \pm 0.02. \tag{3.38}$$

We summarize the experimental constraints used in our fits in Table III, listing the relevant references with each.

C. Direct search mass limits

The absence of sparticle or Higgs boson production at current collider searches for supersymmetric particles puts lower bounds on their possible masses [44]. We veto any pMSSM points that violate the limits. The limits are derived from various experiments that usually *a priori* assume the validity of a chosen model (usually the CMSSM). Where possible, we use more appropriate model independent limits upon sparticle masses coming from searches. SUSY particles may be pair produced at colliders that have sufficient energy, then undergo subsequent decay into SM particles and neutralino LSP. Hard jets or leptons associated with missing energy coming from the neutralino then constitute SUSY direct search signatures. Constraints on sparticle of mass m are often dependent upon the mass difference $\Delta m = m - m_{\rm LSP}$, which is correlated with the energy of visible sparticle decay products [24,98]. The sparticle mass limits derived then depend on this energy, depending upon whether Δm is low (5–10 GeV) or higher. The mass limits we impose on the sparticles and the lightest Higgs boson are summarized in Table IV [44].

A recent random scan study of the pMSSM [33] found that a CDF/D0 bound [99,100] was quite restrictive on their pMSSM parameter-space random sample points when the relic density constraint was applied only as an upper bound (i.e. allowing for additional extra-MSSM sources of dark matter). The bound states that, for $m_{\tilde\chi^\pm_1} - m_{\tilde\chi^0_1} \le 50$ MeV, $m_{\tilde\chi^\pm_1} \ge 206|U_{1w}|^2 + 171|U_{1h}|^2$ GeV at 95% confidence level. Here $|U_{1w}|$ and $|U_{1h}|$ are the Wino and Higgsino content of the lightest chargino, respectively. We did not use this bound in our MULTINEST sampling procedure, but we have checked retrospectively that it would not have significantly changed our fits since only less than 1% of the posterior probability density fails this constraint.

D. Sampling procedure

In this section we summarize the Bayesian inference elements (briefly reviewed in Sec. II) for the pMSSM and the sampling procedure we employ for fitting it to the indirect collider and cosmological data. All of the pMSSM parameters, θ, listed in Table II, are varied simultaneously, our calculation being driven by MULTINEST and the high energy physics software mentioned in the following paragraphs. MULTINEST is described in the Appendix.

Each point is passed in SUSY Les Houches Accord (SLHA) format [101] to the different particle physics software we use to predict the observables described in Sec. III B. For each set of parameters MULTINEST selects, the following steps are followed:

(1) The (input) parameters are passed to `SOFTSUSY2.0.18` [39], which produces the MSSM sparticle masses and couplings. Unphysical points are flagged by the program to have one or some combination of the following properties: absence of electroweak symmetry breaking, the presence of a tachyon, a nonperturbative point where the calculation can no longer be trusted, or the lack of numerical convergence (which usually occurs close to a boundary of good electroweak symmetry breaking). If any of these properties are flagged, then the point is discarded before any further computations and the parameter point is given a zero likelihood. In addition to this, sparticle spectra that violate mass limits, shown in Table IV, from sparticle searches or that have a non-neutralino LSP are also discarded.

(2) Physical parameter points are passed in SLHA format to `micrOMEGAs3.2` [64–67], which calculates the neutralino dark matter relic density, the branching ratio $\mathrm{BR}(B_s \to \mu^+\mu^-)$, and the anomalous magnetic moment of the muon δa_μ. The physical point is then passed to the computer program `SuperIso2.0` [77] and other subroutines. The former calculates $\mathrm{BR}(B \to X_s\gamma)$ and the isospin asymmetry in B meson decays Δ_{0-}, while the latter computes the B-physics ratios $R_{B_u\to\tau\nu}$ and $R_{\Delta M_{B_s}}$.

(3) We then use `SUSYPOPE` [53,54] to calculate the W-boson mass m_W, the effective leptonic mixing angle variable $\sin^2\theta^{\mathrm{lep}}_{\mathrm{eff}}$, the total Z-boson decay width Γ_Z, and the other electroweak physics observables listed in Table III to two loops.

The various physical observables described in Sec. III B, which are derived from the input parameters, form the data set D_i, $i = 1, \ldots, 19$:

$$\mathbf{D} = \{m_W, \sin^2\theta^{\mathrm{lep}}_{\mathrm{eff}}, \Gamma_Z, \delta a_\mu, R^0_l, A^{0,l}_{fb}, A^l = A^e, R^0_{b,c}, A^{b,c}_{fb}, A^{b,c}, \mathrm{BR}(B \to X_s\gamma), \mathrm{BR}(B_s \to \mu^+\mu^-), \Delta_{0-}, R_{\mathrm{BR}(B_u\to\tau\nu)}, R_{\Delta M_{B_s}}, \Omega_{\mathrm{CDM}}h^2\}. \tag{3.39}$$

For each predicted value O_i of observable D_i, the corresponding likelihood is

$$P(D_i|\boldsymbol{\Theta}, H) = \frac{1}{\sqrt{2\pi\sigma_i^2}} \exp\left[-\frac{(O_i - \mu_i)^2}{2\sigma_i^2}\right], \tag{3.40}$$

where μ_i and σ_i are the experimental central values and errors given in Table III. We assume that the observables are independent and combined the likelihoods to

$$L(\boldsymbol{\Theta}) = P(\mathbf{D}|\boldsymbol{\Theta}, H) = \prod_{i=1}^{19} P(D_i|\boldsymbol{\Theta}, H) L_{\mathrm{BR}(B_s\to\mu^+\mu^-)}, \tag{3.41}$$

where $L_{\mathrm{BR}(B_s\to\mu^+\mu^-)}$ is the likelihood value for the indicated observable (see Fig. 1). The predictions from the physical points, as enumerated above, are checked against experimental values and the deviations from this are quantified by the individual likelihood functions Eq. (3.40). The likelihoods from the different observables are combined into one overall likelihood, Eq. (3.41), which is then multiplied by the prior probability density Eq. (2.7) to produce posterior probability density Eq. (2.1).

E. Computer resources

We end this section with the presentation of an estimate of the computing resources used. In the MULTINEST1.3 algorithm we used 4000 live points (see the Appendix and [29,30] for details) and more than 8.6×10^6 likelihood evaluations for the linear prior and more than 2.1×10^7 for the log prior cases. The overall number of likelihood evaluations in this work is more than 2.5×10^8. The computing was performed by 79 twelve-hour jobs at the *Darwin* cluster of the high performance computing service (HPC) at the University of Cambridge. Each run used 128 threads or CPUs. We also used around 40 eight-hour jobs at COSMOS (the U.K. Cosmology supercomputer at DAMTP). At COSMOS each run used 64 CPUs. The total run time adds to more than 15 CPU years. However, the efficiency of the more recent version of MULTINEST has improved, and these computations could take about half of the stated time.

IV. RESULTS AND ANALYSIS

We now present the results of the global fit for the weak-scale pMSSM parameters to indirect collider and cosmological data. We first give the marginalized one-dimensional posterior probability distributions for the 25 parameters and sparticle masses in Sec. IV A. The observable posterior PDFs are discussed in Sec. IV B. In Sec. IV C we present an implementation of Bayesian model selection by comparing two different pMSSM hypotheses, each with either sign of the μ parameter. We address the case of fine-tuning in the pMSSM parameters in Sec. IV D.

Results and analysis on neutralino dark matter and its direct detection prospects are presented in Sec. V. A gen-

eral feature of the results is that they exhibit some amount of prior dependence. This is clearly shown for the case of the amount of fine-tuning in the parameters in Sec. IV D, the muon anomalous magnetic moment (see the δa_μ plots in Fig. 4), and the dominant neutralino dark matter annihilation/coannihilation channels addressed in Sec. V. It is expected that more precise and direct data from the Tevatron and/or the LHC would lift the prior dependence. However, interestingly enough, some of the results, such as the mass of the lightest *CP*-even Higgs boson mass, are very similar for the different priors considered.

A. Parameters and sparticle mass posterior PDFs

Our assumptions about the pMSSM priors are presented in Sec. III A. The priors are updated using the set of different experimental measurements explained in Sec. III B via Bayes' theorem (see Sec. II A). A measure of the amount of information in the likelihood can be seen from the results of the sampling procedure in the form of posterior PDFs. One-dimensional marginalized posterior PDFs of the parameters are shown in Fig. 2. Most of the scalar mass terms in the log prior scenario are much reduced with respect to the corresponding mass term in the linear prior scenario, as expected. Changes to the scalar mass priors (in the log prior case) do change the posterior PDFs of M_1 and M_2. This is because the dark matter likelihood is driving the fit, and dark matter coannihilation requires the mass of the lightest neutralino (controlled by the smaller of M_1 and M_2) to be close to that of the scalar that it is coannihilating with (see Sec. V B for discussion on the coannihilations in the pMSSM). On the other hand, M_3 shows approximate prior independence. For linear priors, upper bounds on the parameters come from a combination of our constraint upon the prior range and the strongly constraining observables (mainly δa_μ) that disfavor heavy sparticle masses. Since M_3 can take either sign, it is on the list of parameters whose prior did not change: therefore, the apparent approximate lack of prior independence is not surprising.[8] M_1, M_2, and M_3 have PDFs that tend to zero as the parameter tends to zero, but a finite bin size means that this may not be evident in plots. Since m_{H_1} and m_{H_2} may take negative values, no logarithm was applied to them in the log-prior case. Thus the apparent prior independence of m_{H_1} is no surprise. The A terms show a peak structure because if their magnitudes are too large, the squark mass becomes tachyonic and thus is disallowed. Radiative corrections to the lightest *CP*-even Higgs mass involving the stops imply that they must be quite heavy, above $\sim$2 TeV in order to push the Higgs mass above its direct search bound. Thus, the log prior only disfavors points at $m_{\tilde{t}_L} = m_{\tilde{b}_L} = 4$ TeV by a factor of 1/2 compared to the lower values. In contrast, other sfermion masses, which may be as low as 200 GeV, obtain a log prior suppression of 1/20 at 4 TeV masses; i.e. the difference between log and linear priors is much more evident in that case. Thus there is no large enhancement of the posterior for small $m_{\tilde{t}_L} = m_{\tilde{b}_L}$, which shows approximately identical posterior PDFs for the two different prior choices.

We display the posterior PDFs of the pole sparticle masses in Fig. 3 along with the posterior PDF of the μ parameter. The mass distributions can be understood from the parameter PDFs discussed above, since there is a rough one-to-one correspondence between the tree-level mass and a mass parameter for many of the sparticles. For the third family sparticles, the A terms and μ parameter contribute via the large mixing, which is proportional to the analogous SM fermion mass. The first and second generation sfermion masses are approximately degenerate, since the degeneracy is only broken by terms of order the second generation fermion mass, negligible compared to the sfermion masses. We see approximate prior independence of $m_{\tilde{t}_1}$, $m_{\tilde{t}_2}$, $m_{\tilde{g}}$, $m_{\tilde{b}_2}$, and $m_A \approx m_H \approx m_{H^\pm}$. Other sfermion masses show the expected log prior suppression at high masses.

The MSSM lightest *CP*-even Higgs mass at tree level is

$$m_h = m_Z |\cos 2\beta|, \tag{4.1}$$

but it receives large radiative corrections from third generation particles, of order 30% of its mass. Since the $\tan\beta$ posterior is similar for both priors, then the tree-level value of m_h will also be similar. An additional small prior dependence comes mainly from $m_{\tilde{t}_R}$ and $m_{\tilde{b}_R}$ prior dependence, but really the model itself constrains the Higgs masses to be largely prior independent. The approximate mass degeneracy in the heavy Higgs masses and little dependence on priors can be seen to originate from the relationships between them. The tree-level MSSM pseudoscalar *CP*-odd Higgs mass is given by

$$m_A^2 = 2|\mu|^2 + m_{H_1}^2 + m_{H_2}^2, \tag{4.2}$$

and it receives quite large radiative corrections. There is only a small prior dependence of m_A, and Eq. (4.2) shows that the approximate prior independence of m_A is something of an accident since $m_{H_2}^2$ and μ show some prior dependence, but this largely cancels in its effect on m_A. Notice that

$$m_H^2 = \frac{1}{2}(m_A^2 + m_Z^2 + \sqrt{(m_A^2 - m_Z^2)^2 + 4m_Z^2 m_A^2 \sin^2(2\beta)}),$$
$$m_{H^\pm}^2 = m_A^2 + m_W^2, \tag{4.3}$$

and since m_A is usually far greater than m_W and m_Z, then $m_A \approx m_H \approx m_{H^\pm}$ holds, although loop corrections contribute to a small nondegeneracy, which, however, is not visible to the eye.

[8]We leave for a future project to understand and analyze the effects that lead to having an upper bound on M_3—.

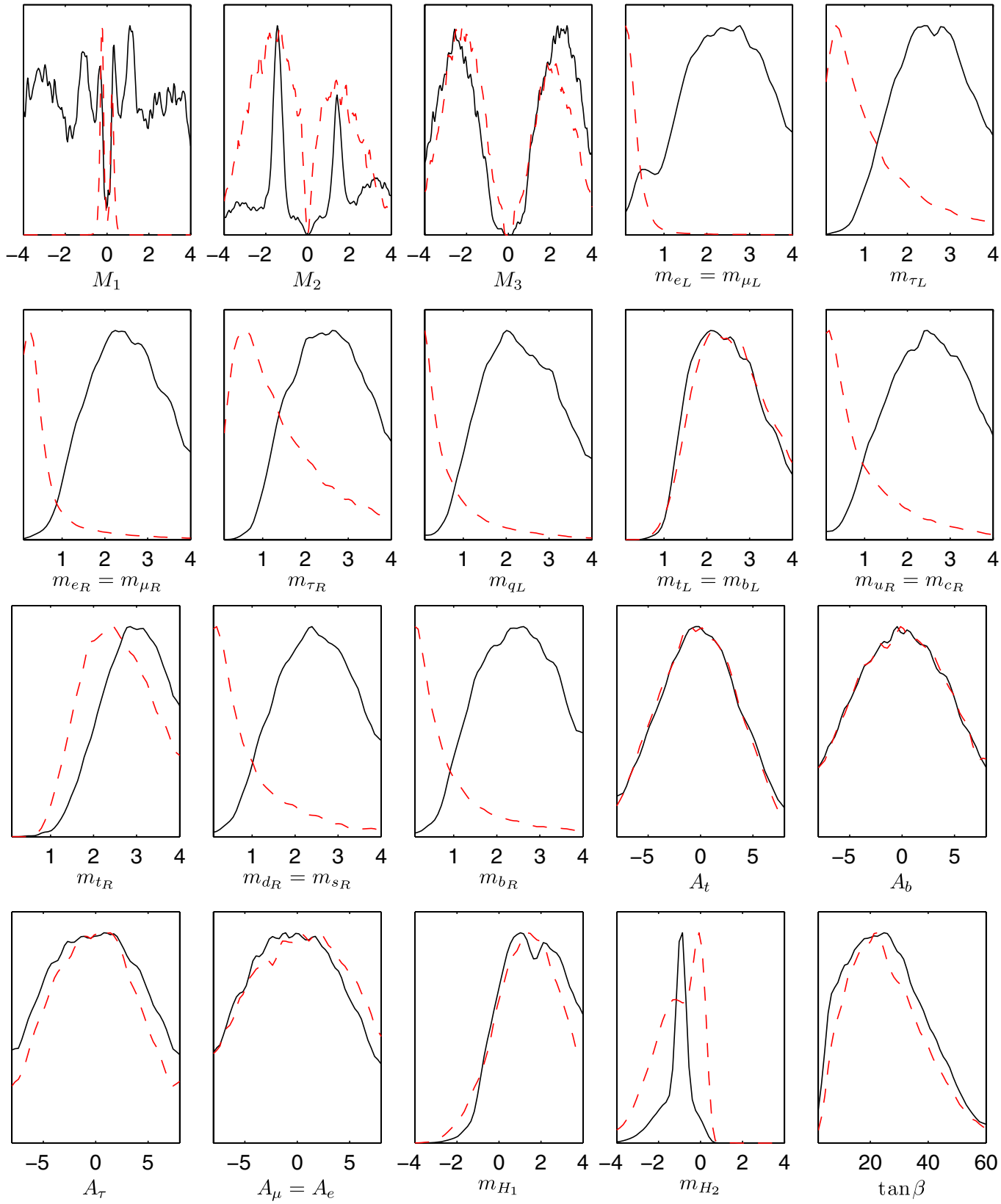

FIG. 2 (color online). Marginalized one-dimensional posterior PDFs for the pMSSM parameters. The soft-breaking scalar mass terms in the log prior scenario (broken lines) are mostly reduced with respect to the corresponding mass term in the linear prior scenario (solid lines). All masses are in TeV units and $m_{q_L} = m_{u_L} = m_{d_L} = m_{c_L} = m_{s_L}$.

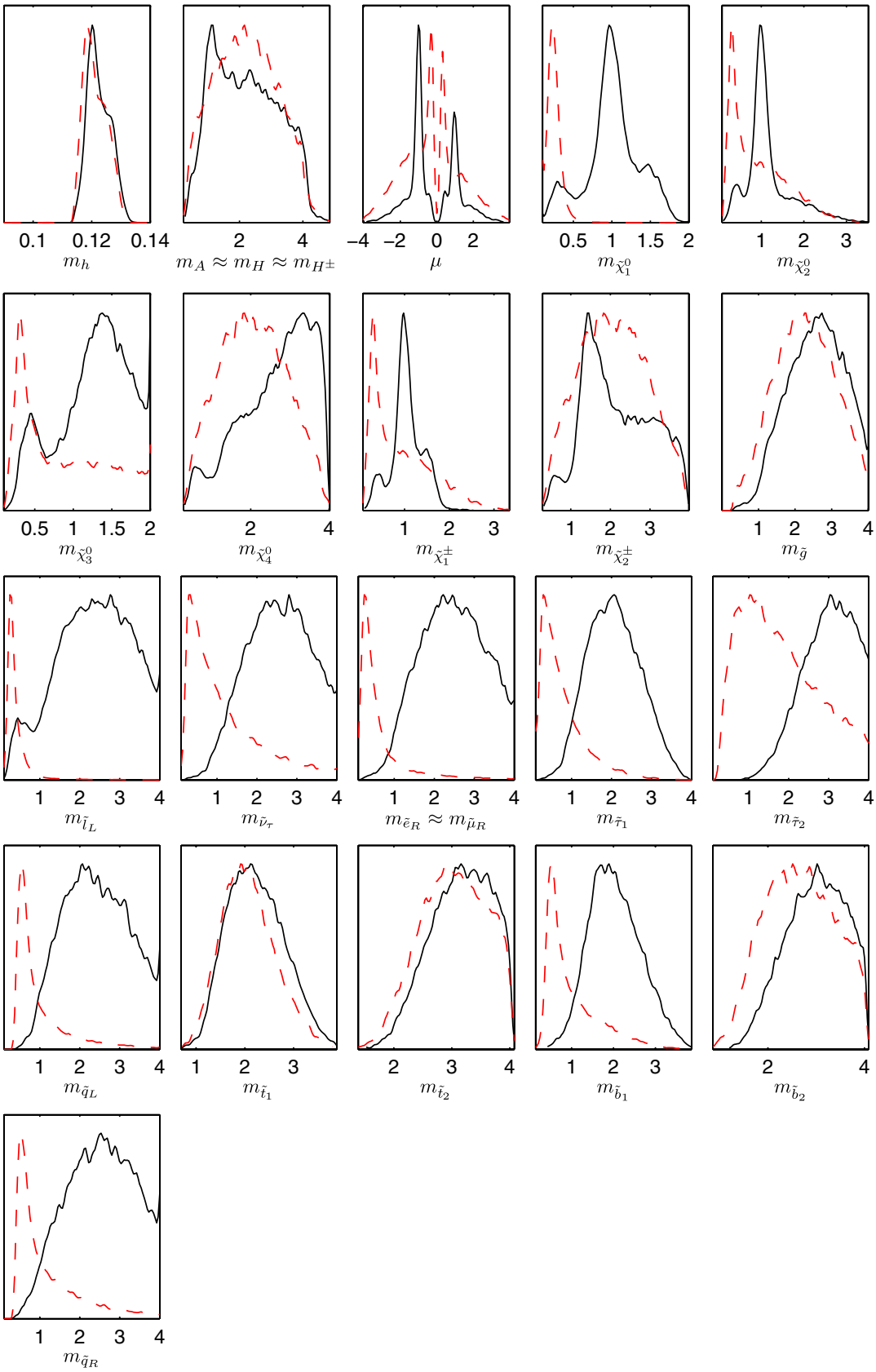

FIG. 3 (color online). Marginalized one-dimensional posterior PDFs for the μ parameter and pMSSM sparticle masses, all in TeV units, for log priors (broken lines) and linear priors (solid lines). First and second generation left-handed sleptons, left-handed squarks, and right-handed squarks are collapsed into single parameters, $m_{\tilde{l}_L}$, $m_{\tilde{q}_L}$, and $m_{\tilde{l}_R}$, respectively.

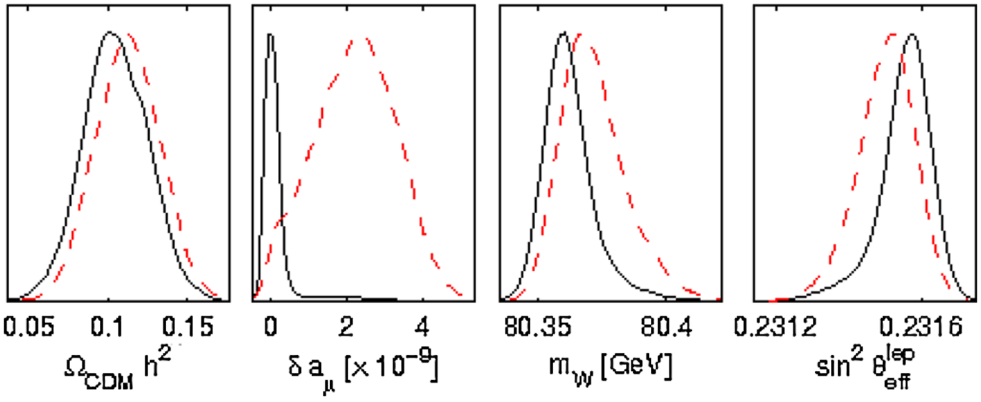

FIG. 4 (color online). Posterior PDF of some of the observables used to constrain the pMSSM. Solid (broken) lines represent plots for the linear (log) prior case. Prior independence is pronounced most in δa_μ. The other observables not shown here are either prior independent or similar to the prior independence in $\Omega_{\rm CDM}h^2$.

B. Observables' PDFs

The observable that most discriminates between the pMSSM fit points is the anomalous magnetic moment of the muon, which is a much better fit for the log prior point, where it receives large corrections from lighter slepton and gaugino masses. m_W and Γ_Z also show a significant difference between the two points, whereas the other observables display only a small difference in statistical pulls. The posterior PDFs for the observables are given in Fig. 4. Differences between the two prior cases are mostly due to the fact that the sparticle mass PDFs are larger in the linear prior, leading to a suppression of SUSY effects in the loops of most observables. The B-physics observables tend to have similar posterior PDFs in the two prior cases. In most of the EWPO, there are larger differences in the posteriors. For δa_μ, there is a particularly large difference between the central values of the linear and log prior PDFs. The leading one-loop gaugino contribution at large $\tan\beta$ is given by [88]

$$\delta a_\mu \approx \frac{m_\mu^2 \mu \tan\beta}{16\pi^2}(g_1^2 M_1 F_1 + g_2^2 M_2 F_2), \tag{4.4}$$

where F_1 and F_2 are positive loop functions proportional to $m_{\rm SUSY}^{-4}$ for the case of degenerate sparticles in the loops. The dominant contributions coming from gauginos and sleptons therefore lead to an enhanced value of δa_μ when they are lighter, as is evident for the log prior fits. As we shall see in Sec. V B the linear prior fits prefer Higgsino exchange to be the dominant LSP annihilation process, as opposed to slepton coannihilation in the log prior case. This occurs at heavier neutralino LSP masses, and hence heavier smuon masses (which are always constrained to be heavier than the neutralino LSP). δa_μ is then relatively badly fit as can be seen in the good-fit point example where the statistical pull is more than 2σ.

C. Sign(μ) comparison

The posterior PDFs in Fig. 3 indicate that the pMSSM prefers $\mu < 0$ compared to $\mu > 0$. This is interesting since in the previous studies of CMSSM $\mu > 0$ was seen to be preferred by the combination of BR($b \to s\gamma$) and δa_μ. One of the statistical tests (a predictive likelihood ratio test) in Ref. [102] found that the two measurements are incompatible in the CMSSM, but the other found no strong evidence for this and so the final conclusion of the analysis remains unclear. The sign of the SUSY contribution to BR($b \to s\gamma$) is dependent upon the sign of μ. There are two dominant SUSY contributions to consider: the first comes from diagrams involving a charged Higgs boson and up-type quarks. The second, involving a chargino and up-type squarks, depends upon the sign of the product $A_t\mu$. Equation (3.25) indicates that there is a preference for a positive total contribution at the 1-σ level. In the CMSSM, A_t is typically negative due to RGE effects. Equation (4.4) shows that the sign of the non-SM contribution to the muon anomalous magnetic moment depends upon the sign of μM_1 and μM_2. In the CMSSM, M_1 and M_2 are positive and so the combination of the $(g-2)_\mu$ and BR($B \to X_s\gamma$) constraints implies a preference for a definite sign of μ. Bayesian analyses [13,34] demonstrated that the current statistical evidence for $\mu > 0$ in the CMSSM is weaker than many may presuppose.

We have not used the freedom to redefine the phases of the fields and make M_2 positive, for example, and so negative M_2 appears in our fits. As such, in the pMSSM both A_t and M_1, M_2 may take either sign, and so the preference for $\mu > 0$ is broken and we may expect that the dominant contributions to the observables do not prefer either sign. On the other hand, there may be some residual dependence from the subdominant contributions, as well as subdominant radiative corrections to other observables. Thus it is still important to check the relative probabilities for sign(μ). For the pMSSM with a linear prior measure we find the following probability for the two signs of μ:

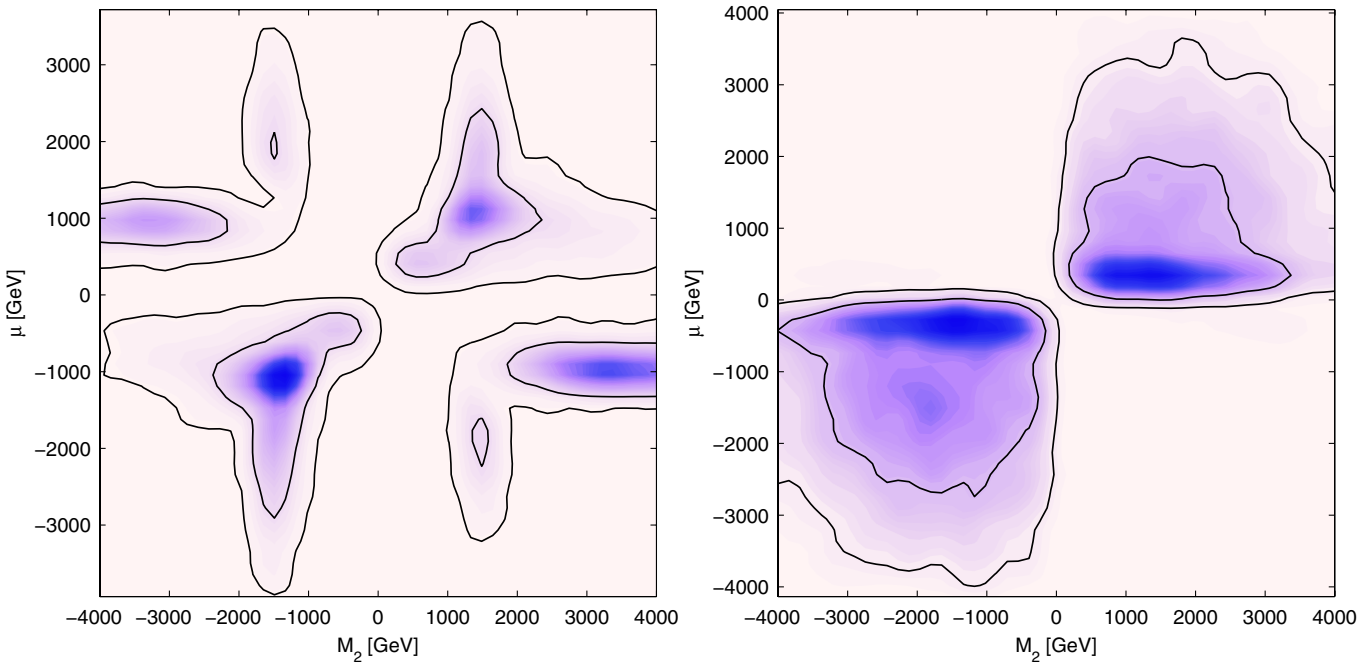

FIG. 5 (color online). Marginalized 2D posterior PDF of M_2 versus μ for a (left) linear prior and (right) log prior. The dark contours show the 68% and 95% Bayesian credibility regions.

$$P(\mu > 0) = 0.40 \pm 0.01 \quad \text{and} \quad P(\mu < 0) = 0.60 \pm 0.01. \tag{4.5}$$

Figure 5 shows the posterior PDF marginalized on the $M_2 - \mu$ plane. The figure shows that, although opposite signs for μ are allowed, it is constrained to have the *same sign* as M_2, especially for log priors where $(g-2)_\mu$ is well fit. For linear priors, the large volume of parameter space leading to heavy sparticle masses mean that this tendency is reduced and there is a small amount of probability that $\mu M_2 < 0$, predicting a small negative δa_μ. Figure 5 clearly shows a symmetry of the fits when one simultaneously flips the signs of M_2 and μ, as should be the case due to phase redefinition freedom.

The SM prediction of $(g-2)_\mu$ remains somewhat controversial. The hadronic contributions that are extracted from τ and e^+e^- data disagree, and one obtains quite different δa_μ constraints depending upon which data set is used. To quantify the extent to which our mild preference for $\mu < 0$ depends on the $(g-2)_\mu$ observable, we made a separate sampling with all except the $(g-2)_\mu$ constraints. We found that $\mu < 0$ is still more probable with

$$P(\mu > 0) = 0.46 \pm 0.02 \quad \text{and} \quad P(\mu < 0) = 0.54 \pm 0.02. \tag{56}$$

Thus, $(g-2)_\mu$ contributes around 0.06 to the probability of $\mu < 0$, the other observables including $\mathrm{BR}(B \to X_s\gamma)$ contributing around 0.04. However, computing the Bayesian evidence ratios in the two scenarios indicate that there are no conclusive evidence, based on Jeffreys scale (see Table I), for one particular sign(μ) over the other. The odds and logarithm of the evidence ratios are summarized in Table V.

D. Fine-tuning

The main motivation of weak-scale SUSY is to solve the technical hierarchy problem, explaining why the Higgs boson remains at the weak scale despite quantum corrections that are as large as the largest mass scale in the theory (e.g. the Planck scale). In order for softly broken SUSY to still provide a resolution of the technical hierarchy prob-

TABLE V. The Bayesian evidence ratios for the pMSSM with $\mu > 0$ and $\mu < 0$ with the linear priors measure. "All observables" refers to all the constraints discussed in Sec. IV B. Z_+ and Z_- represent the evidence for the hypothesis for the linear prior pMSSM with $\mu > 0$ and with $\mu < 0$, respectively. A prior probability of 0.5 is assigned to each hypothesis.

Data considered	$\lvert\log_e \Delta E\rvert$	Odds, Z_+/Z_-	Remark
All constraints	-0.41 ± 0.04	0.67 ± 0.03	Inconclusive
All minus $(g-2)_\mu$ constraints	-0.18 ± 0.04	0.84 ± 0.04	Inconclusive

lem, the SUSY-breaking terms should not be much larger than the TeV scale; otherwise *a priori* unnatural cancellations between radiative corrections are required in order to keep the Higgs boson mass low. Direct SUSY search limits imply lower bounds on sparticle masses, which already start to imply that the MSSM parameters must cancel somewhat in order to separate the electroweak and SUSY-breaking scales. This is termed the ''little hierarchy problem'' [103,104] (see a recent discussion in [105]). We wish to quantify the necessary amount of fine-tuning in the pMSSM parameters needed to make the setup consistent with the imposed sparticle mass bounds.

We follow the approach in [106], quantifying the amount of fine-tuning in the Z-boson mass prediction coming from Higgs potential minimization conditions. We consider this as a measure of fine-tuning in the pMSSM. The tree-level Z-boson mass is given by

$$m_Z^2 = -m_{H_1}^2\left(1 - \frac{1}{\cos 2\beta}\right) + m_{H_2}^2\left(1 + \frac{1}{\cos 2\beta}\right) - 2|\mu|^2, \tag{4.7}$$

where

$$\sin 2\beta = \frac{2m_3^2}{m_{H_1}^2 + m_{H_2}^2 + 2|\mu|^2}. \tag{4.8}$$

The amount of fine-tuning is quantified by considering the sensitivity of m_Z to a variation of a parameter ξ [107]:

$$\Delta(\xi) = \left|\frac{\partial \log m_Z^2}{\partial \log \xi}\right|, \tag{4.9}$$

where $\xi = m_{H_1}^2$, $m_{H_2}^2$, m_3^2, and μ are the relevant parameters in the pMSSM. Assuming $\tan\beta > 1$, from Eqs. (4.7), (4.8), and (4.9), one derives

$$\begin{aligned}
\Delta(\mu) &= \frac{4\mu^2}{m_Z^2}\left(1 + \frac{m_A^2 + m_Z^2}{m_A^2}\tan^2 2\beta\right),\\
\Delta(m_3^2) &= \left(1 + \frac{m_A^2}{m_Z^2}\right)\tan^2 2\beta,\\
\Delta(m_{H_1}^2) &= \left|\frac{1}{2}\cos 2\beta + \frac{m_A^2}{m_Z^2}\cos^2\beta - \frac{\mu^2}{m_Z^2}\right|\\
&\quad\times\left(1 - \frac{1}{\cos 2\beta} + \frac{m_A^2 + m_Z^2}{m_A^2}\tan^2 2\beta\right),\\
\Delta(m_{H_2}^2) &= \left|-\frac{1}{2}\cos 2\beta + \frac{m_A^2}{m_Z^2}\sin^2\beta - \frac{\mu^2}{m_Z^2}\right|\\
&\quad\times\left|1 + \frac{1}{\cos 2\beta} + \frac{m_A^2 + m_Z^2}{m_A^2}\tan^2 2\beta\right|.
\end{aligned} \tag{4.10}$$

$\Delta(\mu)$, $\Delta(m_3^2)$, $\Delta(m_{H_1}^2)$, and $\Delta(m_{H_2}^2)$ are added in quadrature to obtain an overall measure of fine-tuning, Δ_T:

$$\Delta_T \equiv \sqrt{\Delta(\mu)^2 + \Delta(m_3^2)^2 + \Delta(m_{H_1}^2)^2 + \Delta(m_{H_2}^2)^2}. \tag{4.11}$$

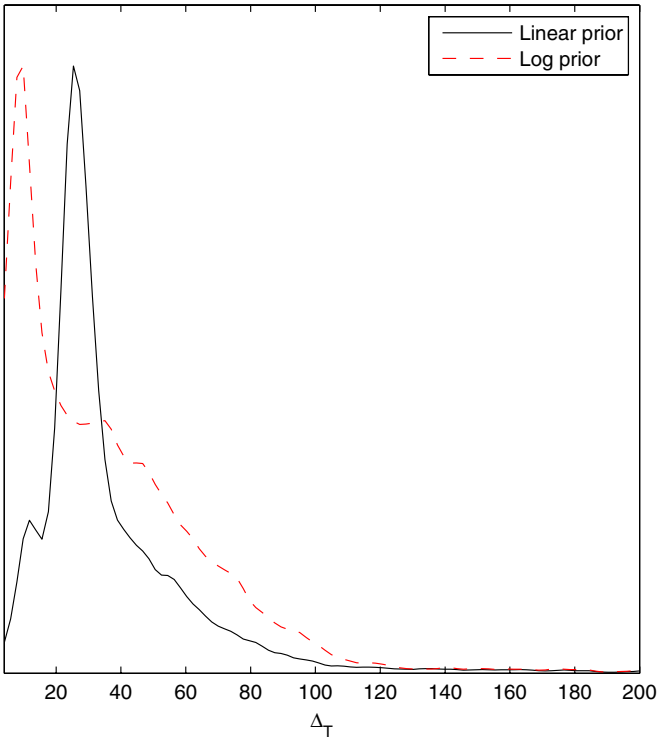

FIG. 6 (color online). Fine-tuning PDFs in the pMSSM.

Values of Δ_T far greater than unity indicate large fine-tuning.

The posterior PDF for the amount of fine-tuning in the pMSSM is shown in Fig. 6. The logarithmic prior scenarios have lower Δ_T than in the linear prior. This is not surprising since the SUSY-breaking terms are much reduced in the former scenarios than in the latter. We see from the figure that the fine-tuning is most likely low at around $\Delta_T \sim$ 20–30, but there is a tail extending beyond $\Delta_T = 100$. One could use a prior of $1/\Delta_T$ to encode a belief in less fine-tuned points in our global fits [11]. Alternatively, one could place a cut on Δ_T, but the value of such a cut is, of course, subjective. Eighty-two percent of the high posterior PDF points, around 4.0×10^4 of samples, have $\Delta_T > 10$, so a hard cut placed at 10 would have a drastic effect on the fits. Here we decline to change the prior or place cuts, since we are content with observing that, for most of the probability mass in the fits, it is not unacceptably large. For the highest likelihood models the fine-tuning is reduced from its average. For example, for the good-fit point in the linear prior sample, $\Delta_T = 24$, whereas for the good-fit point in the log prior sample, $\Delta_T = 27$.

Notice that in general the amount of fine-tuning we find is small compared to previous studies of the MSSM that start at a high scale, running down to the TeV scale using the RG equations. The reasons for this include, as explained in Refs. [104,108], that the amount of fine-tuning is a function of the cutoff scale and tends to decrease with this scale because the interval of RG running of the soft parameters induces electroweak symmetry breaking at tree

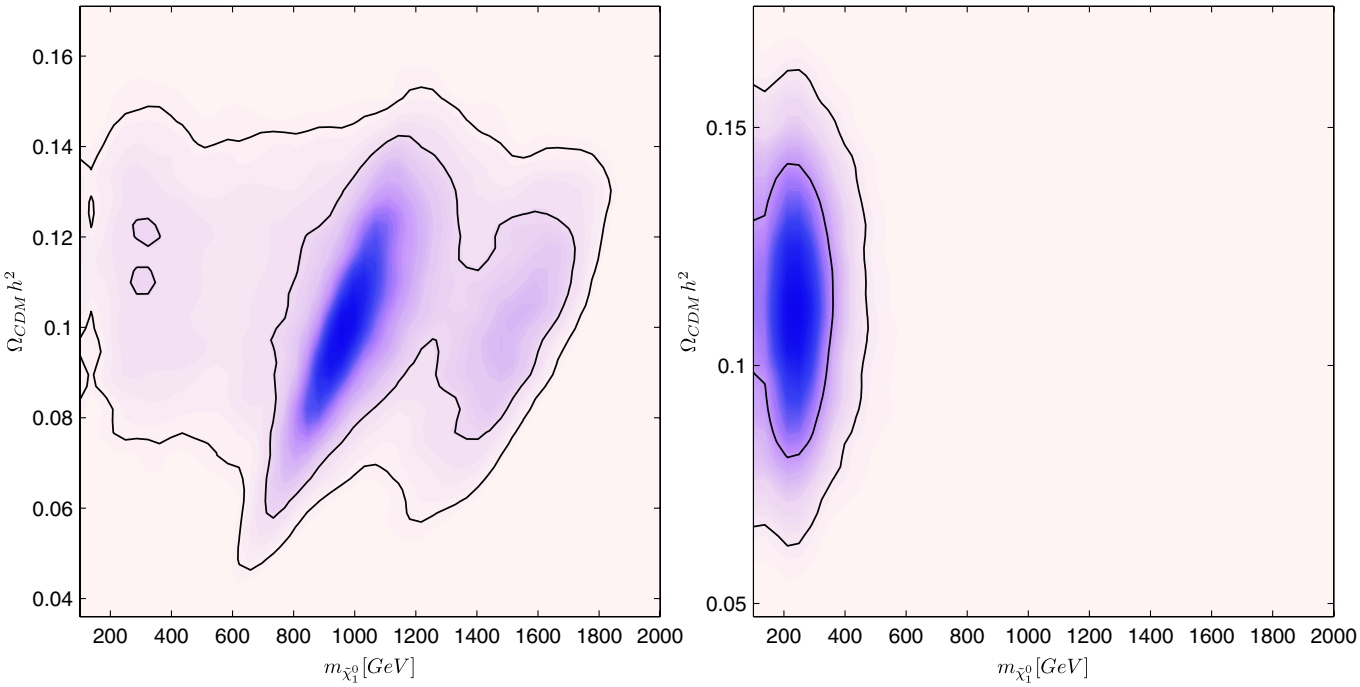

FIG. 7 (color online). Marginalized two-dimensional posterior PDFs of the predicted neutralino dark matter relic density ($\Omega_{\mathrm{CDM}}h^2 = \Omega_{\chi_1^0}h^2$) from spectra points that pass all constraints) against the neutralino mass. Linear priors are on the left-hand side and log priors on the right. The dark contours show the 68% and 95% Bayesian credibility regions. Note that the feature shown toward the left-hand side of the linear prior plot is due to the peak in the neutralino mass at around 200 GeV in Fig. 3, which here just makes it into the 68% region.

level and the cross talk (through RG running) between parameters in the Higgs sector and those from the squarks, gluinos, etc., sectors is drastically reduced such that the latter parameters can be much heavier than m_Z without disturbing the naturalness of the electroweak scale.[9] Reference [108] found some approximate seminumerical solutions of the RGEs for the case that the boundary conditions on SUSY-breaking parameters are set at the GUT scale $\sim 10^{16}$ GeV. The dominant term in $\Delta(\mu(M_{\mathrm{GUT}}))$ typically comes from cross talk with the GUT scale gluino mass $M_3(M_{\mathrm{GUT}})$:

$$\Delta(\mu(M_{\mathrm{GUT}})) = a(\tan\beta)\frac{M_3^2(M_{\mathrm{GUT}})}{M_Z^2}, \qquad (62)$$

where the authors determined the coefficient $a(\tan\beta)$ numerically: $a(2.5) = 24$ and $a(10) = 12$, for example. This is to be contrasted with the pMSSM in Eq. (4.10), where the terms in $\Delta(\mu)$ are set at the SUSY-breaking scale and are $\sim O(1)$, and does not involve the gluino mass, upon which there are strong empirical lower bounds.

[9]We thank J. R. Espinosa for interesting conversations on this point and on fine-tuning in general.

V. NEUTRALINO DARK MATTER

Assuming R-parity conservation, the LSP may be a good dark matter (DM) candidate. In Ref. [25], a pMSSM study of the ability of SUSY measurements at future colliders to constrain dark matter properties was considered. We assume that the neutralino LSP constitutes the DM in the universe. The DM relic density then depends upon the LSP mass and, through its composition in terms of gauginos and Higgsino, its interactions. Two-dimensional marginalized posterior PDFs showing preferred regions in the relic density versus LSP mass are shown in Fig. 7. There is a mild positive correlation between the preferred mass and the dark matter relic density $\Omega_{\mathrm{CDM}}h^2$ for linear priors that is not evident for the log priors. It is clear that the LSP mass is not well constrained by current data, since it is highly prior dependent. The nature of the neutralino LSP in the pMSSM is addressed in Sec. V A. The mass difference between the LSP and the next-to-lightest supersymmetric particle (NLSP) is important because if it is small, the LSP may efficiently coannihilate, in the early universe, with the NLSP, significantly reducing the relic density. The different possible NLSPs in the pMSSM with the corresponding posterior probabilities are listed in Sec. V B. The dominant (co-)annihilation channels are presented in Sec. V B. We present the prospects of direct dark matter detection in Sec. V C.

A. Neutralino dark matter composition

The nature of the neutralino LSP determines the (dominant) processes by which it (co-)annihilates into SM particles and therefore affects its present number density. This was illustrated using the randomly scanned pMSSM samples in [4] where it was shown that the nature of the neutralino LSP depends upon whether one assumes that the LSP makes up all or only some of the DM relic density. The neutralino mass matrix is given by $\frac{1}{2}\psi^{0T} M_N \psi^0 + \text{H.c.}$ where $\psi^{0T} = (-i\tilde{b}, -i\tilde{w}^3, \tilde{H}_1^0, \tilde{H}_2^0)$,

$$M_{\rm N} = \begin{pmatrix} M_1 & 0 & -m_Z c_\beta s_W & m_Z s_\beta c_W \\ 0 & M_2 & m_Z c_\beta c_W & -m_Z s_\beta c_W \\ -m_Z c_\beta s_W & m_Z c_\beta c_W & 0 & -\mu \\ m_Z s_\beta s_W & -m_Z s_\beta c_W & -\mu & 0 \end{pmatrix}, \tag{5.1}$$

$c_x = \cos x$, and $s_x = \sin x$. The neutralino mass eigenstates are $\tilde{\chi}_i^0 = N_{ij}\psi_j^0$ where N is a unitary transformation that diagonalizes M_N. The LSP neutralino mass eigenstate is therefore a mixture of bino, wino, and Higgsino:

$$\tilde{\chi}_1^0 = N_{11}\tilde{b} + N_{12}\tilde{w}^3 + N_{13}\tilde{H}_1^0 + N_{14}\tilde{H}_2^0. \tag{5.2}$$

Different regions of parameter space give different neutralino LSP compositions. When $M_1 \ll \min(M_2, |\mu|)$, $N_{11} \sim 1$, and the LSP is dominantly bino. Bino LSPs give a relic density that is too high for most of the parameter space unless some specific mechanism (such as efficient coannihilations or annihilations through a resonance) is working. When $M_2 < \min(M_1, |\mu|)$, N_{12} dominates; i.e. the LSP is dominantly wino and is quasi-mass degenerate with the lightest chargino. This leads to strong coannihilations between the LSP and the chargino, and typically the relic density is much smaller than the WMAP constraint for wino LSPs. For $|\mu| < \min(M_1, M_2)$, N_{13} and N_{14} are of order one and the LSP is dominantly Higgsino, and there may be efficient annihilations into top and weak gauge boson pairs. In the Higgsino-dominated LSP scenario, $\tilde{\chi}_1^0$, $\tilde{\chi}_2^0$, $\tilde{\chi}_1^\pm$ are almost all mass degenerate and are Higgsino-like. Of course, there exist mixed cases that include several of these limiting behaviors.

The gaugino/Higgsino mixture PDF of the LSP is shown in Fig. 8 constructed from the fraction

$$Z_g = |N_{11}|^2 + |N_{12}|^2$$

following [109]. The expression $1 - Z_g$ is unity if the neutralino LSP is fully Higgsino-like and zero if fully gauginolike. The plot shows that LSP is mostly Higgsino in the linear prior case, similar to the nonuniversal Higgs mass scenario [110], and mostly gaugino for the log prior scenario. Thus, current data do not unambiguously constrain the LSP content. The good-fit point from the linear prior sample has a mixed wino-Higgsino LSP (more precisely, the point has $|N_{13}| \sim |N_{14}| = 0.7$ and $N_{12} = 0.15$). The log prior sample good-fit point has a bino dominated LSP ($|N_{11}| = 0.998$), but there are several light sparticles, allowing sufficient annihilation.

B. (Co-)Annihilations

At early times of the universe the LSP is in thermal equilibrium with other particles and, ignoring for now coannihilations, its number density evolution is governed by the Boltzmann equation

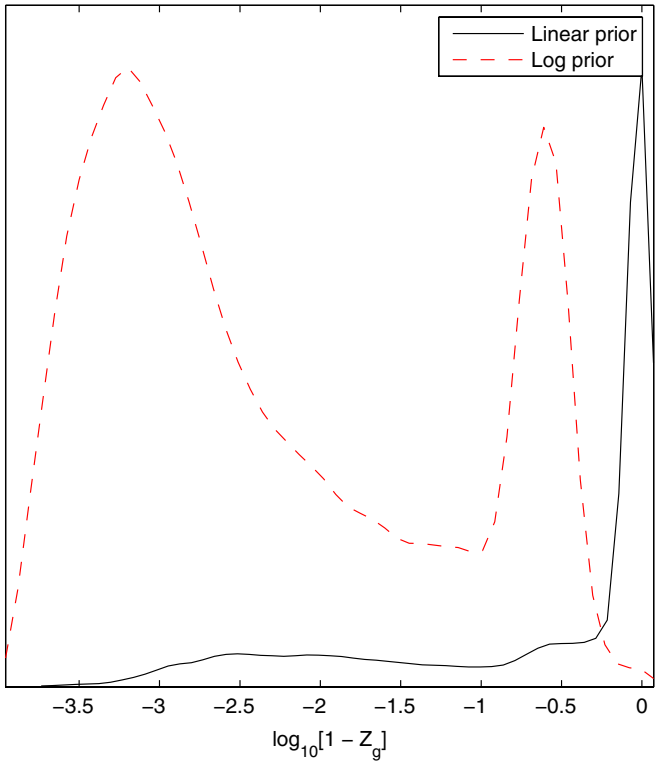

FIG. 8 (color online). pMSSM neutralino gaugino-Higgsino admixture fractions. Higgsino domination is at the right-hand side of the plot and gaugino domination is at the left-hand side. The chosen scale on the horizontal axis better shows the structure of the curves especially the double peaks in the log prior case. The linear prior samples turned out to be mostly Higgsino-like, unlike the log prior case where the neutralino samples are mostly gauginolike but also significantly Higgsino-like. This is due to lower sparticle masses in the log prior pMSSM that allow various channels for the neutralino annihilation and coannihilations.

$$\frac{dn_{\tilde{\chi}_1^0}}{dt} = -3Hn_{\tilde{\chi}_1^0} - \langle\sigma v\rangle\{n^2_{\tilde{\chi}_1^0} - (n^{\rm eq}_{\tilde{\chi}_1^0})^2\}. \quad (5.3)$$

Here H is the Hubble expansion rate of the universe, $n_{\tilde{\chi}_1^0}$ is the number density, and $\langle\sigma v\rangle$ is the thermally averaged annihilation cross sections of the neutralino LSP. v is the relative velocity of the annihilating pair. The LSP annihilation rate is given by $\Gamma_{\tilde{\chi}_1^0} = \langle\sigma v\rangle n_{\tilde{\chi}_1^0}$. At a freeze-out temperature T_f, the neutralino decouples, $\Gamma_{\tilde{\chi}_1^0} = H(T_f)$. Substituting $H(T_f)$ into Eq. (5.3) predicts that the LSP relic density is inversely proportional to the thermally averaged annihilation cross section, $\langle\sigma v\rangle$. This means that for the LSP relic abundance today to be in the WMAP-5 range, Eq. (3.38), there must be a significant number of annihilations of the neutralino LSP at earlier times. The possible processes are mostly two-particle final states that could be a fermion–antifermion pair, combinations of the weak gauge bosons ($W^{\pm}$, Z^0), or combinations of the Higgs bosons (h^0, H^0, A^0, $H^{\pm}$) (see e.g. [111]). The discussion becomes much more involved once coannihilation processes are taken into account, since coupled Boltzmann equations are required for each relevant SUSY particle species.

Coannihilation processes dominate in parameter-space points with NLSP that are almost mass degenerate with the LSP. At such points the neutralino abundance also depends strongly on the annihilations of the NLSPs [112,113] and the number densities of the LSPs and NLSPs are coupled. A review of different coannihilation studies was presented in [4]. Here we present and analyze the outcome of the pMSSM annihilation and coannihilation results for our two different prior measures. We shall only discuss processes that contribute 1% or more of the annihilation cross section.

In Table VI we give a list of possible NLSPs and corresponding posterior probabilities for each. The probabilities indicate that neutralino-chargino coannihilations are most likely to be dominant in the pMSSM with a linear prior measure. For the log prior measure, neutralino-slepton coannihilations are the most probable. The dominant channels for the linear prior sample good-fit point are direct neutralino-chargino coannihilation and neutralino annihilation via chargino exchange into Z- and W-boson pairs. For the log prior measure good-fit point, the dominating channels are neutralino coannihilations with various sleptons. Many different processes contribute at the percent level. We present the identities of the dominant channel, along with its posterior probability in Table VII. The most likely channel is neutralino-chargino coannihilation for the linear prior and neutralino annihilation for the log prior. From the large prior dependence in the results, we deduce that current data are not sufficient to constrain the dark matter annihilation properties of the LSP.

TABLE VI. pMSSM NLSP identity probabilities for linear and log priors.

NLSP	$P(\text{NLSP})_{\text{Linear}}$	$P(\text{NLSP})_{\text{Log}}$
$\tilde{\chi}_2^0$	14%	1%
$\tilde{\chi}_1^{\pm}$	77%	15%
$\tilde{g}$	1%	0%
$\tilde{\nu}_e$	2%	39%
$\tilde{\nu}_\tau$	0%	4%
$\tilde{e}_L$	0%	2%
$\tilde{e}_R$	0%	27%
$\tilde{\tau}_1$	0%	7%
$\tilde{u}_L$	1%	1%
$\tilde{u}_R$	1%	1%
$\tilde{s}_R$	1%	1%
$\tilde{t}_1$	1%	0%
$\tilde{b}_1$	1%	1%

TABLE VII. Posterior probabilities for dominant annihilation and coannihilation channels.

(Co-)annihilation	Linear prior case	Log prior case
$\tilde{\chi}_1^0\tilde{\chi}^{\pm}$	35%	5%
$\tilde{\chi}_1^0\tilde{\chi}_1^0$	20%	28%
$\tilde{\chi}_1^0\tilde{\chi}_2^0$	0%	7%
$\tilde{\chi}_1^0$ sleptons	0%	23%

C. Direct detection

Many different experiments search for the nature of dark matter (e.g. see [114], and references therein). Indirect detection experiments are designed to observe the annihilation products of dark matter particles. We do not address indirect detection here and save it for future consideration. Here, we consider direct detection experiments such as XENON [115], CDMS [116,117], ZEPLIN [118,119], Edelweiss [120], CRESST [121], WARP [122,123], or COUPP [124]. Such experiments are designed to observe the elastic scattering of dark matter particles with nuclei. The LSP may interact with quarks in target nuclei via t-channel CP-even Higgs (or Z-boson) exchange or s-channel squark exchange and with gluons via squark loop contributions. DM direct detection rates also depend on the local neighborhood DM density and velocity distribution. The density, which is estimated to lie between 4×10^{-25} g/cm^{-3} and 13×10^{-25} g/cm^{-3} (0.22–0.73 GeV/cm^3), is inferred by fitting observations to models of galactic halo [125,126]. The velocity is expected to be around 230 ± 20 km/s [127]. More modern halo profiles exist but give densities ranging in the large range taken to model theoretical uncertainties. We ask the reader to bear this factor of 3 uncertainty on the density (and therefore the rate) in mind when interpreting plots.

The elastic scattering cross section is partitioned into spin-dependent and spin-independent components. The spin-independent part is currently the most constraining,

and we concentrate on it. It is proportional to the square of the target nucleus atomic number, A^2. This enhancement is because the dark matter wavelength is of the same order as the size of a nucleus and hence the scattering amplitudes on individual nucleons add coherently. There is one experimental claim in direct detection experiments of a signal in the annual modulation rate [128]. This result has not been confirmed by other experiments and would be incompatible with a neutralino LSP candidate, so we do not use it to constrain the pMSSM. Aside from this, no positive signal has been detected to date in dark matter detection experiments. A positive signal would constrain SUSY parameter space if one assumed a particular local neighborhood DM density and velocity distribution.

The spin-independent neutralino-nucleus elastic scattering cross section is given by

$$\sigma \approx \frac{4m^2_{\tilde{\chi}^0_1} m^2_T}{\pi(m_{\tilde{\chi}^0_1} + m_T)^2}([Zf_p + (A - Z)f_n]^2 + [a^V_u(A + Z) + a^V_d(2A - Z)]^2/64), \quad (5.4)$$

where m_T is the mass of the target nucleus and Z and A are the atomic number and atomic mass of the nucleus, respectively. f_p and f_n are the neutralino's couplings to protons and neutrons, given by [129]

$$f_{p,n} = \sum_{q=u,d,s} f^{(p,n)}_{T_q} a_q \frac{m_{p,n}}{m_q} + \frac{2}{27} f^{(p,n)}_{TG} \sum_{q=c,b,t} a_q \frac{m_{p,n}}{m_q}, \quad (5.5)$$

a_q and $a^V_{u,d}$ are, respectively, the scalar and vector neutralino-quark couplings [129–134], and $f^{(p,n)}_{T_q}$ denote the quark content of the nucleon. They have been experimentally bounded to be $f^{(p)}_{T_u} \approx 0.020 \pm 0.004$, $f^{(p)}_{T_d} \approx 0.026 \pm 0.005$, $f^{(p)}_{T_s} \approx 0.118 \pm 0.062$, $f^{(n)}_{T_u} \approx 0.014 \pm 0.003$, $f^{(n)}_{T_d} \approx 0.036 \pm 0.008$, and $f^{(n)}_{T_s} \approx 0.118 \pm 0.062$ [135–137]. The first term in Eq. (5.5) corresponds to interactions with the quarks in the target, which can occur through either t-channel CP-even Higgs exchange, or s-channel squark exchange. The second term corresponds to interactions with gluons in the target through a quark/squark loop. $f^{(p)}_{TG}$ is given by $1 - f^{(p)}_{T_u} - f^{(p)}_{T_d} - f^{(p)}_{T_s} \approx 0.84$, and analogously, $f^{(n)}_{TG} \approx 0.83$. The vector coupling part in Eq. (5.4) is important for Higgsino-like LSP where the interaction is mostly via Z-boson exchange.

The direct detection constraints from the cryogenic cold dark matter search (CDMS) experiments on the pMSSM is shown in Fig. 9. The large prior dependence of the results indicates that current data are insufficient to constrain the direct detection cross sections. One can say that there is clearly a wide allowed range for the direct detection cross sections.

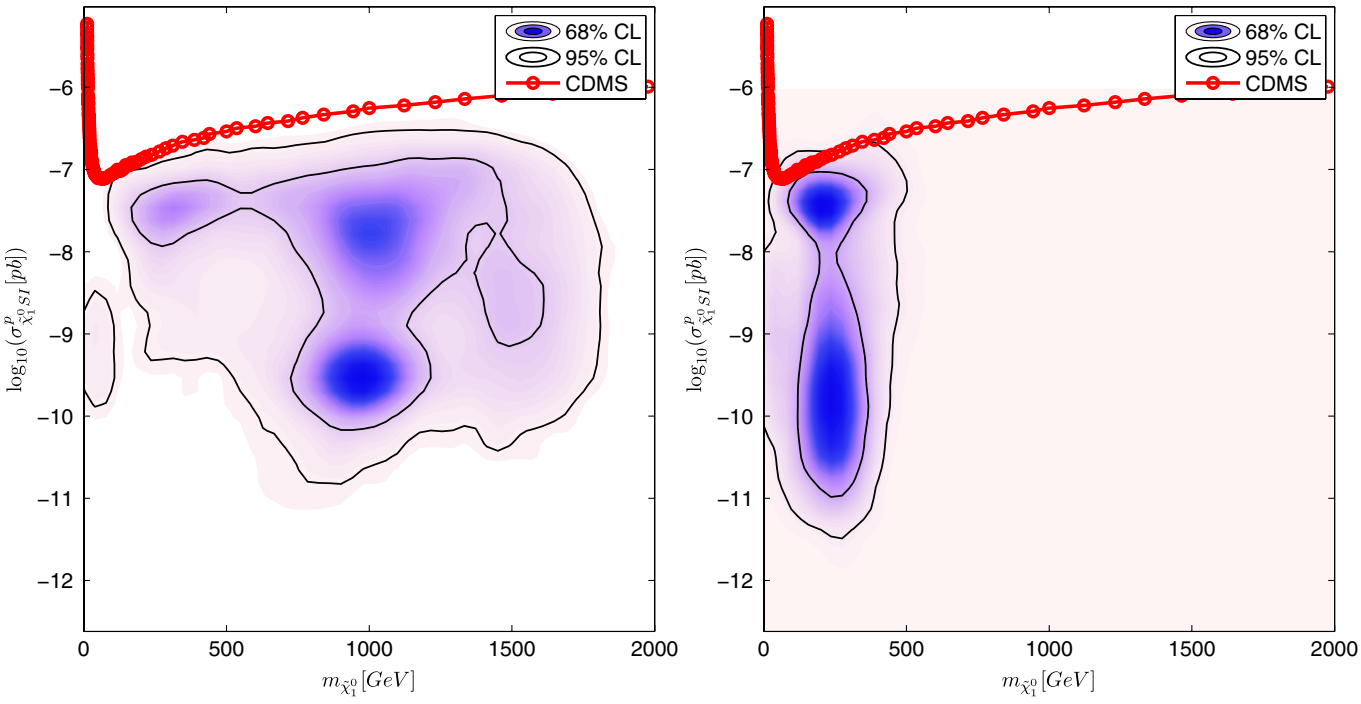

FIG. 9 (color online). Posterior PDF of the neutralino-proton spin-independent scattering cross section for the pMSSM with linear (left) and log (right) prior measures. The CDMS 90% confidence level upper bound is also shown, assuming a local DM density of 0.3 GeV/cm^3. The dark contours show the 68% and 95% Bayesian credibility regions.

D. Relaxing the purely LSP dark matter assumption

The analysis presented above was done assuming that the neutralino LSP is the only source of dark matter. It is known that the LSP relic density is sensitive to the assumed cosmology. For example, big bang nucleosynthesis expansion rates can enhance the calculated relic density without affecting other important cosmological quantities [138]. The inclusion of right-handed neutrinos could change the relic density prediction; see, for instance, [139]. One could also allow for additional non-neutralino dark matter components. In order to see the potential effect of such model changes, we relax the constraint from the DM relic density to the case where only $\Omega_{\rm CDM}h^2$ predictions larger than the central values are penalized according to the following likelihoods (shown in Fig. 10):

$$L_{\rm CDM}(\Omega_{\rm CDM}) = \begin{cases} \frac{1}{\mu + \sqrt{\pi s^2/2}}, & \text{if } \Omega_{\rm CDM} < \mu, \\ \frac{1}{\mu + \sqrt{\pi s^2/2}} \exp[-\frac{(\Omega_{\rm CDM}-\mu)^2}{2s^2}], & \text{if } \Omega_{\rm CDM} \geq \mu, \end{cases} \tag{5.6}$$

where $\mu = 0.1143$ is the experimental central value quoted above and s is an inflated error on relic density that includes theoretical uncertainties in its prediction.

We have made an independent run using Eq. (5.6), i.e. relaxing the purely LSP DM assumption, i.e. implicitly assuming some other component of dark matter. We wish to examine the amount of DM that comes from the LSP. These runs were performed in Ref. [32], where the relevant constraints can be found. Linear priors were used on the parameters, which had a 2 TeV upper bound. We find in Fig. 11 that the preferred relic density is low compared with the purely LSP DM assumption: around $\Omega_{\rm CDM}h^2 = 10^{-2}$–$10^{-3}$. Thus once one allows for an additional component of DM to the LSP, the model prefers the additional component to dominate the relic density.[10]

VI. CONCLUSIONS AND OUTLOOK

We have presented the first statistically convergent global fit of the pMSSM model with its 25 independent continuous parameters plus a discrete parameter, $\text{sign}(\mu) = \pm$, to the dark matter relic density, indirect observables, and direct sparticle search constraints. We have used the entire set of relevant electroweak precision observables and B-physics data, as well as the anomalous magnetic moment of the muon as indirect observables.[11] The evidence for the linear and log prior measure pMSSM in light of the data is $\log_e Z = 63.211 \pm 0.033$ and $\log_e Z = 65.043 \pm 0.042$, respectively. We give the evidence values since they are useful to compare other models to: if a different model's properly normalized evidence is calculated with similar data to those we have used, the model may be compared to the pMSSM. We have presented good-fit points in the pMSSM parameter space.

This work constitutes a technical demonstration that statistically convergent global fits in high dimensions involving curving degeneracies and several modes are now feasible. This feasibility is due to new sampling algorithms and improvements in the speed of computation and access to it. It allows more complete phenomenological studies of multiparameter models beyond the standard model that could not have been completed in the past. In particular, the setup and techniques employed here provide an unbiased approach to MSSM phenomenology—independent of the underlying theory, the mechanism to break SUSY or its mediation—hence it could lead to more robust SUSY phenomenological studies and guides for LHC SUSY searches and for dark matter search experiments. As ex-

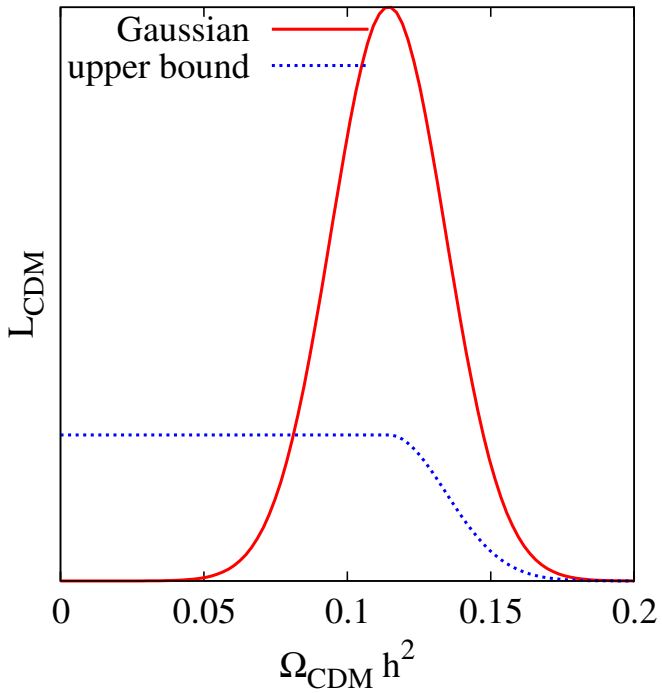

FIG. 10 (color online). Depiction of the likelihood constraint on the predicted value of $\Omega_{\rm DM}h^2$ due to the lightest neutralinos, compared to a simple Gaussian with WMAP5 central value and a 1σ uncertainty of 0.02 used in the rest of the paper.

[10]Some of us hope to return to this issue in future work. We thank Bryan Webber for suggesting this comparison.

[11]If the reader is interested in accessing the pMSSM data (sample points), please contact S. AbdusSalam or B. Allanach.

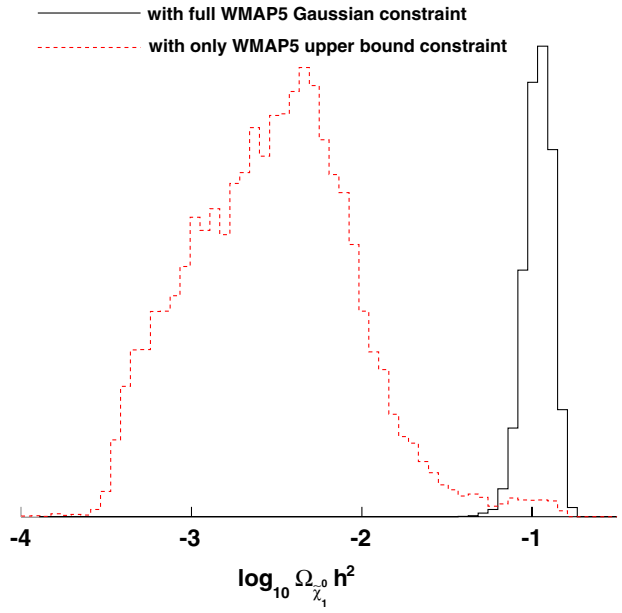

FIG. 11 (color online). Neutralino relic density assuming WMAP5 as a Gaussian likelihood constraint or as an upper bound. For this plot only, a 2 TeV range linear pMSSM with other parameters as in Ref. [32] was taken.

pected, the results of this exercise differ significantly from those of the more studied CMSSM/mSUGRA, and thus the pMSSM parameter space provides a much richer and appropriate arena for LHC studies of the MSSM.

For the analysis we consider prior measures either flat in the parameters (a linear prior) or flat in the logarithm of the parameters (a log prior) in order to check robustness of inferences. Given the large number of (the pMSSM) parameters compared with the (weak constraining power of the) data available at the moment, it is very interesting that indeed there are some prior-independent results or inferences. The lightest *CP*-even Higgs boson mass and the stop masses fall into this category of robust and prior-independent results. The other sparticle masses and all dark matter properties exhibit significant prior dependence and require more direct and precise data (or more constrained models) to make their prediction robust. We emphasize that prior dependence is present and it is a positive feature of Bayesian methods, since its absence signals when there are enough data to make the fits robust. This can be used as a guideline for future studies of the experimental implications of the MSSM. In particular, if SUSY is discovered via sparticle production at colliders and many sparticle properties are precisely measured, it will be possible to use the techniques showcased in the present work to extract pMSSM information. Such information can then be checked for consistency with more constrained models.

We now contrast our methods with the recent random points scan analysis of the pMSSM in Ref. [33] and a similar earlier work in Ref. [4]. These works perform a pMSSM random parameter scan to find points that pass direct search and dark matter constraints while being within 2σ of the central values of some indirect constraints. All such points are considered on an equal footing, and as such (as emphasized by the authors) are not a statistical global fit. We, on the other hand, allow a tradeoff between different observables in a statistically correct fashion; one may tolerate a moderately bad fit in one observable if it fits the other observables particularly well. Our use of Gaussian distributions for the likelihoods (instead of the 2σ top-hat function in [4,33]) is justified by the central limit theorem and the maximum entropy principle [140]. Interesting points with LHC phenomenology not covered by previous studies of constrained models were found in Ref. [33], which was the main aim of the approach (a few thousand points passed the constraints, out of $\sim 10^7$ scanned). We aim to perform a complete and statistically convergent global fit of the pMSSM. To achieve this we take advantage of the power of the MULTINEST algorithm, which provides samples in moderately high dimensional parameter spaces (with curving degeneracies and different modes) much more efficiently than in random/grid parameter scans. In [33] there was more emphasis on direct search limits, which are more sophisticated than the ones employed in the present paper. Since the sparticle masses implied by our fits are large, our results are insensitive to the exact form of the direct search limits. The density of points in Ref. [33] also shows prior dependence although the results were not interpreted statistically (and thus they were not Bayesian nor frequentist). Another major difference to our approach is that in Ref. [33], the WMAP constraint is used only as an upper bound (making viable points much easier to find) and so the existence of another non-MSSM dark matter particle is assumed. This changes the character of the points: allowing MSSM points that predict approximately zero LSP relic density means that a large number of sampled points have a wino dominated LSP. We, however, assume in most of our analysis that the neutralino constitutes all of the dark matter. In Sec. V D we presented an independent run made using the WMAP constraint only as a lower bound, and our results (as expected) agree with those of [4,33] in the sense that, in that case, the LSP contribution tends to be only a small fraction of the total dark matter.

There are many directions in which this research could be extended. For each of the tens of thousands of preferred points in our sample, a detailed calculation of LHC observables, such as inclusive counts of opposite sign dilepton and trilepton events, could be made using standard event generators and detector simulators, as has been done for more constrained models such as the CMSSM [141]. This would provide a portrait of the signature space that may eventually be useful in direct SUSY searches. On a simpler level, one could compute relative probabilities of various sparticle mass hierarchies. The indirect dark matter

detection prospects could also be evaluated, although with current data they are likely to be highly prior dependent. The impact of the inclusion of the fine-tuning into the prior could be analyzed. Assuming a particular parameter point, the impact of LHC SUSY measurements on our fits could be evaluated, and an estimate of how much luminosity would be required in order to make inferences approximately prior independent.[12] In this case, model comparison between more constrained models and the pMSSM could be informative. One could determine, for a given LHC luminosity, which models could be made prior independent. The extension of the analysis to the full 124 MSSM parameter space may still be out of reach at the moment. Algorithms improving the MULTINEST algorithm may be required before attempting it. An extension of this work to include reasonable generalizations of the minimal flavor violation scenario adding a few extra parameters should be possible. Also, including R-parity violation to the pMSSM as well as a phenomenological NMSSM are within reach of the techniques we used here. Some of us hope to return to these issues in future work.

ACKNOWLEDGMENTS

We would like to thank Arne Weber for help with fixes to the code SUSYPOPE, A. Pukhov for help with micrOMEGAs, N. Mahmoudi for help with SuperIso, and M. Dolan for checks with the likelihood code. We thank S. Abel, J. Conlon, D. J. C. MacKay, J. R. Espinosa, S. Krippendorf, C. Lester, M. Gomez-Reino, F. Marchesano, P. Slavich, K. Suruliz, A. Uranga, B. Webber, and E. Witten for useful discussions. The calculations performed in this paper were done using the Cambridge High Performance Computing Cluster (HPC) *Darwin* and COSMOS, the U.K. National Cosmology Supercomputer. We thank Andrey Kaliazin, Stuart Rankin, and Victor Travieso for assistance in setting and running the codes on these computing facilities and John Turner and the HPC group for important assistance regarding the rights to use HPC. This research was partially funded by STFC. S. S. A. is supported by the Gates Cambridge Trust and thanks the African Institute for Mathematical Sciences (AIMS) for hospitality during the early stages of this work. F. Q. thanks the organizers of the Cooks Branch 2009 meeting for hospitality during the last stages of this work.

APPENDIX: NESTED SAMPLING AND THE MULTINEST ALGORITHM

For scanning parameter spaces of large dimensionality we have to use efficient modern approaches for sampling the posterior. In such problems, interesting parameter regions are often tiny in some directions, and many directions are orthogonal to ones along which the likelihood is degenerately high. In this section we present the procedure, in the context of the pMSSM, for the Monte Carlo technique called nested sampling developed by Skilling [31] and implemented in MULTINEST. It is a general method for evaluating the integral Eq. (2.2) from which representative samples from the posterior distribution Eq. (2.1) are obtained as by-product. The method differs from the traditional approach to inference dating back to Metropolis *et al.* (1953) [143] where the emphasis is more on evaluating the posterior density than in calculating the evidence. Skilling's method goes as follows. Exploring the 25-dimensional coordinate $\mathbf{\Theta}$ to evaluate the evidence integral is impractical. Instead, the prior mass $dX = \pi(\mathbf{\Theta})d\mathbf{\Theta}$ can be used directly to convert the 25-dimensional into a one-dimensional integral over a unit interval. Let $X(L)$ be the prior mass enclosed within the likelihood contour, $L(\mathbf{\Theta}) = L$ in the parameter space. That is,

$$X(L) = \int_{L(\mathbf{\Theta})>L} \pi(\mathbf{\Theta})d^{25}\mathbf{\Theta}. \tag{A1}$$

As L increases from zero to infinity, the enclosed prior mass decreases from $X(0) = 1$ to $X(\infty) = 0$. The inverse function $L(X) \equiv L$ is the contour value (a likelihood value) such that the volume enclosed is X (see Fig. 12 for an illustration). Equation (A1) and the definition of its inverse implies that the evidence Eq. (2.2) can be expressed as

$$Z = \int L(\mathbf{\Theta})\pi(\mathbf{\Theta})d^{25}\mathbf{\Theta} = \int_0^1 L(X)dX. \tag{A2}$$

Given the likelihood values $L_i = L(X_i)$ at a sequence of m points $0 < X_m < \cdots < X_2 < X_1 < X_0 = 1$, the evidence is estimated as a weighted sum,

$$Z = \sum_{i=1}^{m} L_i w_i, \tag{A3}$$

where for the trapezoidal rule $w_i = \frac{1}{2}(X_{i-1} - X_{i+1})$.

1. Evidence evaluation

The nested sampling procedure for evaluating the evidence starts with the accumulation of N points uniformly drawn from the prior, the initialization of the evidence, $Z = 0$, and the initialization of the prior volume, $X_0 = 1$. The number, N, of "live" points, $\mathbf{\Theta}_1, \ldots, \mathbf{\Theta}_N$ is preserved throughout the procedure and every point is associated with its corresponding likelihood value: $L(\mathbf{\Theta}_1), \ldots, L(\mathbf{\Theta}_N)$. Each step $i = 1, 2, 3, \ldots$ over the iterations is associated with the lowest likelihood L_i (or the largest prior mass, X_i) that defines the contour line (or shell) $L(\mathbf{\Theta}) = L_i$ over parameter space. For moving from the $(i-1)$th to the ith iteration a new point is drawn from the set of points uniformly distributed in $(0, X_{i-1})$, the parameter-space region with likelihoods $L \geq L(X_i) = L_i$.

[12] A Bayesian approach has recently been used to ameliorate the LHC inverse problem in the MSSM by combining LHC data with indirect observables [142].

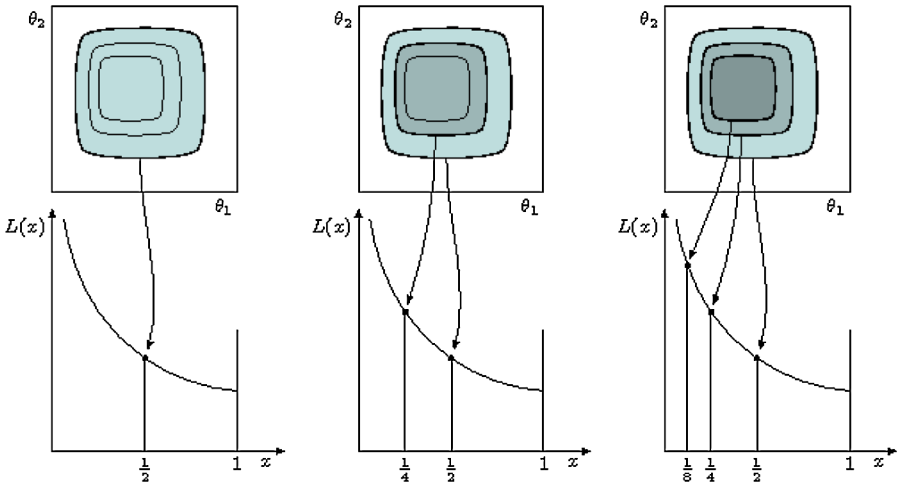

FIG. 12 (color online). Likelihood contours over a toy two-parameter space showing the enclosed volume mapped to corresponding prior mass. A prior mass $x = \frac{1}{2}$ is mapped to the likelihood contour that encloses $\frac{1}{2}$ of the prior volume. Note the nested nature of the contour lines. Figures are from [37].

This is illustrated in Fig. 13. The new point replaces the one with the lowest likelihood. X_i is set to $X_i = \exp(-i/N)$, the weight w_i to $\frac{1}{2}(X_{i-1} - X_{i+1})$, and the evidence Z incremented by $L_i w_i$. This procedure is repeated for the subsequent iterations.

The prior volume shrinkage ratios $t_i = X_i/X_{i-1}$ are distributed according to $\Pr(t_i) = N t_i^{N-1}$ in $(0, 1)$ where t_i is the largest of N random numbers uniformly distributed in $(0, 1)$. Sampling over t represents a geometrical exploration of the parameter space. The mean and standard deviation of t are

$$E(\log t) = -\frac{1}{N} \quad \text{and} \quad \sigma[\log t] = \frac{1}{N}, \tag{A4}$$

respectively. This justifies the assignment $X_i = \exp(-i/N)$ since each draw of $\log t$ is independent, and after i iterations of the sampling procedure the prior volume will shrink down according to

$$\log X_i \approx -(i \pm \sqrt{i})/N. \tag{A5}$$

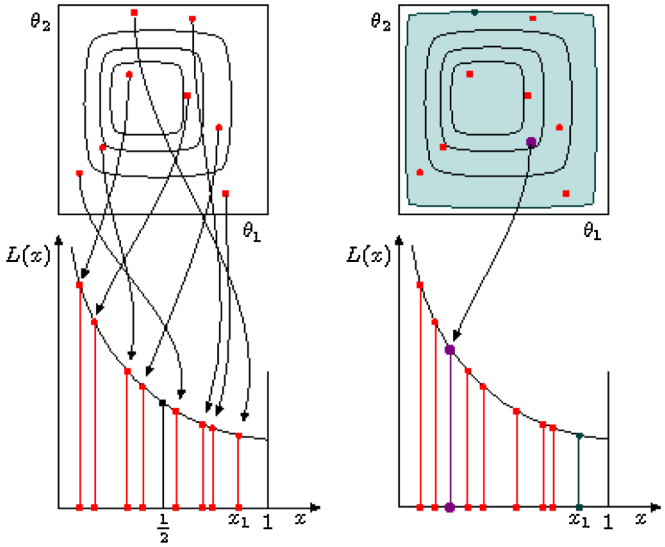

FIG. 13 (color online). The left shows $N = 8$ live points uniformly distributed in parameter space [or prior volume space $(0, 1)$] and sorted according to corresponding likelihood values. On the right is a picture illustrating the sampling of a new point (big purple) dot from the live points uniformly distributed in $(0, x_1)$. Figures are from [37].

2. Stopping criterion

The nested sampling procedure is terminated after a preset number of the iterations (as described in Sec. A 1) or when the largest likelihood taken over the whole currently (at the instance of check for termination, say, the jth iteration) available prior mass would not increase the evidence value by more than some preset fraction f (we use 0.5 in log evidence). That is, the procedure is terminated if

$$\max(L(\mathbf{\Theta}_1), \ldots, L(\mathbf{\Theta}_N))X_j < f Z_j.$$

The integration Z is dominated around the region $X \approx e^{-H}$, wherever the bulk of the posterior mass is to be found. Here

$$H = \text{information} = -\int \log(dX/dP)dP$$
$$\approx \sum_i \log\left(\frac{L_i}{Z}\right)\frac{L_i w_i}{Z}, \tag{A6}$$

and dX/dP is the compression ratio representing the frac-

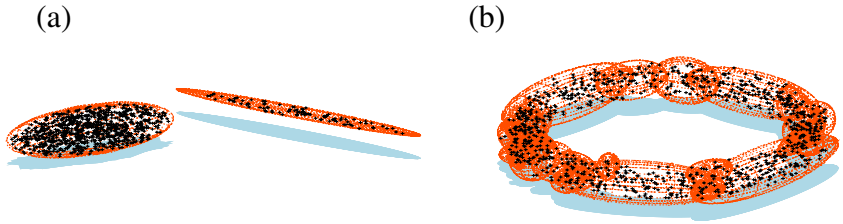

FIG. 14 (color online). The ellipsoidal decompositions performed by MULTINEST. The points given as input are overlaid on the resulting ellipsoids. One thousand points were sampled uniformly from the following: (a) two nonintersecting ellipsoids; and (b) a torus.

tion of the prior mass that contains the bulk of the posterior. $dP = p(\mathbf{\Theta})d\mathbf{\Theta} = Z^{-1}L(\mathbf{\Theta})\pi(\mathbf{\Theta}), d\mathbf{\Theta}$. Recalling that $X_i \approx e^{-i/N}$, we expect the integration procedure to take $NH \pm \sqrt{NH}$ steps (iterations) before reaching covering the bulk of the posterior. Hence another termination condition could be to continue iterating until the count i is significantly greater than NH.

The uncertainty in X translates to a geometrical uncertainty factor $\exp(\pm\sqrt{H/N})$ in the weights w_i of the dominating iterates. This in turn gives the uncertainty in the evidence via Eq. (A3) as $\mathrm{dev}(\log Z) \approx \sqrt{H/N}$ so that

$$\log Z = \log\left(\sum_{i=1}^{m} L_i w_i\right) \pm \sqrt{\frac{H}{N}}. \tag{A7}$$

3. Posterior inferences

The posterior distribution $p(\mathbf{\Theta})$ is simply the prior distribution weighed by the likelihood. This can be trivially extracted from the evidence calculation since the set of sampled points $\mathbf{\Theta}_1, \ldots, \mathbf{\Theta}_N$ is already a posterior representative provided it is assigned the appropriate importance weight and normalized by the evidence Z to produce probability density with unit total. That is, at the ith iteration the posterior probability density is

$$p_i = \frac{L_i w_i}{Z}. \tag{A8}$$

These are generated from the sequences of discarded points (the points with the lowest likelihood value at each iteration) during the sampling procedure. From these posterior sequence properties such as the mean μ and standard deviation σ of some $Q(\mathbf{\Theta})$ are easily computable:

$$\mu = \sum_i p_i Q(\mathbf{\Theta}_i) \quad \text{and} \quad \mu^2 + \sigma^2 = \sum_i p_i Q(\mathbf{\Theta}_i)^2. \tag{A9}$$

Equally weighed samples selected proportionally to p_i can be used to construct marginalized posterior distributions in $\mathbf{\Theta}$.

For completeness, it is worth mentioning that there are alternative methods for evaluating the evidence with other advanced MCMC algorithms like thermodynamic integration and it is not clear yet which method is best for high dimensional problems[13]: dimensions greater than 10. However, for this paper we implement the nested sampling algorithm for our purpose using the MULTINEST code [29], which has the additional quality of being efficient in sampling multimodal posteriors exhibiting curving degeneracies (see a summarized account in Sec. A 4).

4. MULTINEST

The most challenging task in implementing the nested sampling algorithm is drawing samples from the prior within the hard constraint $L > L_i$ at each iteration i. Employing a naive approach that draws blindly from the prior would result in a steady decrease in the acceptance rate of new samples with decreasing prior volume (and increasing likelihood). The MULTINEST algorithm [29,30] tackles this problem through an ellipsoidal rejection sampling scheme by enclosing the live point set into a set of (possibly overlapping) ellipsoids, and a new point is then drawn uniformly from the region enclosed by these ellipsoids. The number of points in an individual ellipsoid and the total number of ellipsoids is decided by an ''expectation-maximisation'' algorithm so that the total sampling volume, which is equal to the sum of volumes of the ellipsoids, is minimized. This allows maximum flexibility and efficiency by breaking up a mode resembling a Gaussian into a relatively fewer number of ellipsoids, and if the posterior mode possesses a pronounced curving degeneracy so that it more closely resembles a (multidimensional) ''banana'' then it is broken into a relatively large number of small ''overlapping'' ellipsoids (see Fig. 14). With enough live points, this approach allows the detection of all the modes simultaneously resulting in typically 2 orders of magnitude improvement in efficiency and accuracy over standard methods for inference prob-

[13]We thank David Mackay for interesting discussions about this. See, for example, http://www.inference.phy.cam.ac.uk/mackay/presentations/nested06/.

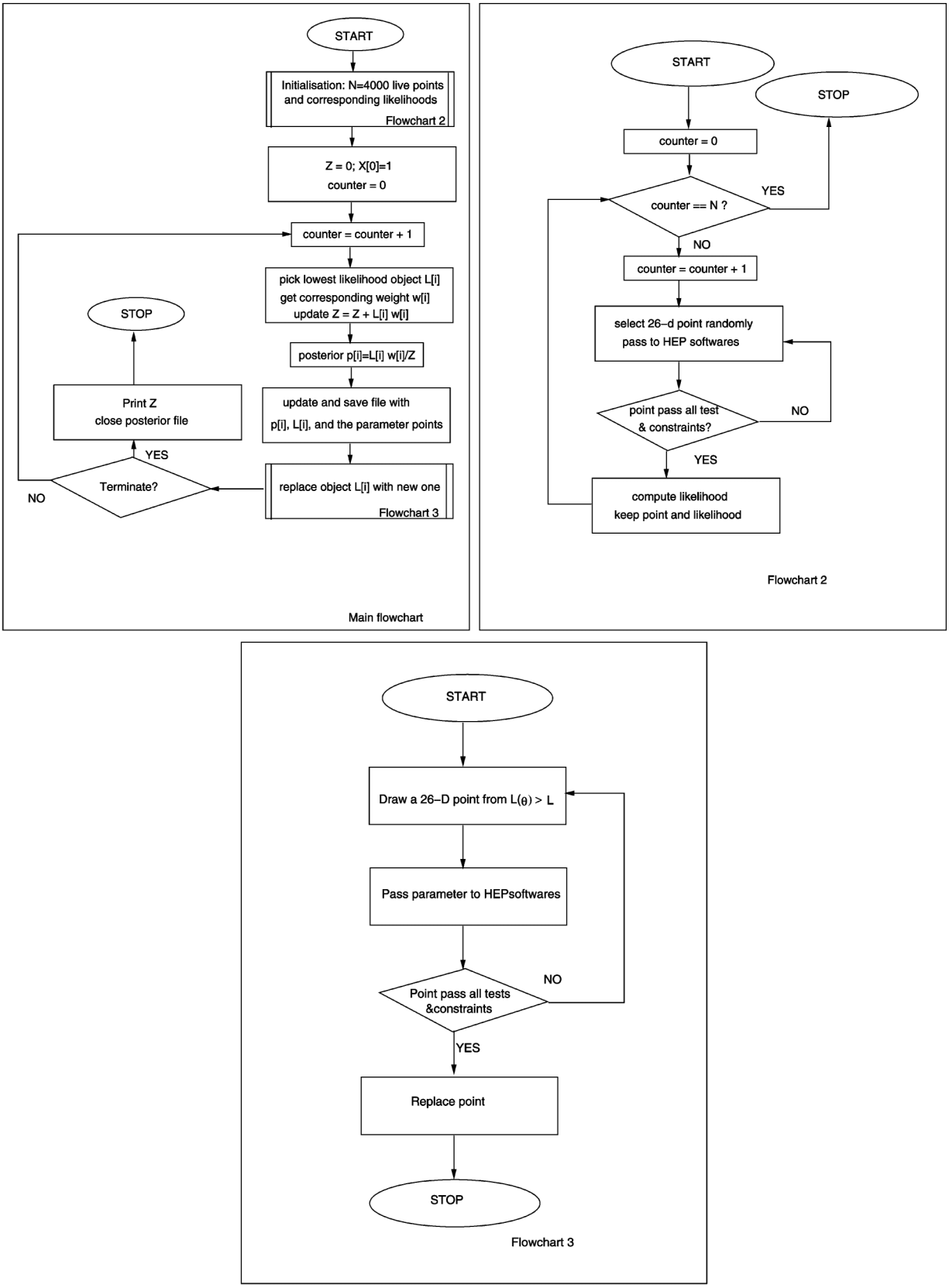

FIG. 15. Flow charts summarizing the sampling procedure: Z refers to the Bayesian evidence, Eqs. (2.2), (A2), and (A3); X_i is the prior mass, Eq. (A1); and p_i is the posterior probability, Eq. (A8). HEP software refers to the different computer programs described in Sec. III D.

lems in cosmology and particle physics phenomenology (see e.g. [32,34,144–146]). The MULTINEST procedure as applied to our pMSSM fits is summarized by the flow charts in Fig. 15.

[1] D. J. H. Chung *et al.*, Phys. Rep. **407**, 1 (2005).
[2] R. L. Arnowitt and P. Nath, Phys. Lett. B **299**, 58 (1993).
[3] J. R. Ellis, K. A. Olive, Y. Santoso, and V. C. Spanos, Phys. Rev. D **69**, 095004 (2004).
[4] S. Profumo and C. E. Yaguna, Phys. Rev. D **70**, 095004 (2004).
[5] E. A. Baltz and P. Gondolo, J. High Energy Phys. 10 (2004) 052.
[6] J. R. Ellis, S. Heinemeyer, K. A. Olive, and G. Weiglein, J. High Energy Phys. 02 (2005) 013.
[7] L. S. Stark, P. Hafliger, A. Biland, and F. Pauss, J. High Energy Phys. 08 (2005) 059.
[8] B. C. Allanach and C. G. Lester, Phys. Rev. D **73**, 015013 (2006).
[9] R. R. de Austri, R. Trotta, and L. Roszkowski, J. High Energy Phys. 05 (2006) 002.
[10] B. C. Allanach, C. G. Lester, and A. M. Weber, J. High Energy Phys. 12 (2006) 065.
[11] B. C. Allanach, Phys. Lett. B **635**, 123 (2006).
[12] L. Roszkowski, R. Ruiz de Austri, and R. Trotta, J. High Energy Phys. 07 (2007) 075.
[13] B. C. Allanach, K. Cranmer, C. G. Lester, and A. M. Weber, J. High Energy Phys. 08 (2007) 023.
[14] O. Buchmueller *et al.*, J. High Energy Phys. 09 (2008) 117.
[15] V. S. Kaplunovsky and J. Louis, Phys. Lett. B **306**, 269 (1993).
[16] A. Brignole, L. E. Ibanez, and C. Munoz, arXiv:hep-ph/9707209.
[17] B. C. Allanach, F. Quevedo, and K. Suruliz, J. High Energy Phys. 04 (2006) 040.
[18] K. Choi, A. Falkowski, H. P. Nilles, and M. Olechowski, Nucl. Phys. **B718**, 113 (2005).
[19] S. S. AbdusSalam, J. P. Conlon, F. Quevedo, and K. Suruliz, J. High Energy Phys. 12 (2007) 036.
[20] B. S. Acharya, K. Bobkov, G. L. Kane, J. Shao, and P. Kumar, Phys. Rev. D **78**, 065038 (2008).
[21] L. Aparicio, D. G. Cerdeno, and L. E. Ibanez, J. High Energy Phys. 07 (2008) 099.
[22] S. Krippendorf and F. Quevedo, J. High Energy Phys. 11 (2009) 039.
[23] B. C. Allanach, M. J. Dolan, and A. M. Weber, J. High Energy Phys. 08 (2008) 105.
[24] A. Djouadi *et al.* (MSSM Working Group Collaboration), arXiv:hep-ph/9901246.
[25] E. A. Baltz, M. Battaglia, M. E. Peskin, and T. Wizansky, Phys. Rev. D **74**, 103521 (2006).
[26] R. Lafaye, T. Plehn, M. Rauch, and D. Zerwas, Eur. Phys. J. C **54**, 617 (2008).
[27] R. Trotta, Contemp. Phys. **49**, 71 (2008).
[28] A. R. Liddle, Annu. Rev. Nucl. Part. Sci. **59**, 95 (2009).
[29] F. Feroz and M. P. Hobson, arXiv:0704.3704.
[30] F. Feroz, M. P. Hobson, and M. Bridges, arXiv:0809.3437.
[31] J. Skilling, in *Nested Sampling*, edited by R. Fischer, R. Preuss, and U. V. Toussaint, American Institute of Physics Conference Series (AIP, New York, 2004), pp. 395–405.
[32] S. S. AbdusSalam, AIP Conf. Proc. **1078**, 297 (2008).
[33] C. F. Berger, J. S. Gainer, J. L. Hewett, and T. G. Rizzo, J. High Energy Phys. 02 (2009) 023.
[34] F. Feroz *et al.*, J. High Energy Phys. 10 (2008) 064.
[35] M. E. Cabrera, J. A. Casas, and R. Ruiz de Austri, J. High Energy Phys. 03 (2009) 075.
[36] R. D. Cousins, Phys. Rev. Lett. **101**, 029101 (2008).
[37] D. J. C. Mackay, *Information Theory, Inference and Learning Algorithms* (Cambridge University Press, Cambridge, U.K., 2003), p. 640, ISBN 0521642981.
[38] S. S. AbdusSalam, B. C. Allanach, M. J. Dolan, F. Feroz, and M. P. Hobson, Phys. Rev. D **80**, 035017 (2009).
[39] B. C. Allanach, Comput. Phys. Commun. **143**, 305 (2002).
[40] S. Dimopoulos and D. W. Sutter, Nucl. Phys. **B452**, 496 (1995).
[41] H. E. Haber, Nucl. Phys. B, Proc. Suppl. **62**, 469 (1998).
[42] A. Djouadi, J.-L. Kneur, and G. Moultaka, Comput. Phys. Commun. **176**, 426 (2007).
[43] S. P. Martin and J. D. Wells, Phys. Rev. D **64**, 035003 (2001).
[44] C. Amsler *et al.* (Particle Data Group Collaboration), Phys. Lett. B **667**, 1 (2008).
[45] CDF Collaboration, arXiv:hep-ex/0703034.
[46] J. Alcaraz *et al.* (ALEPH Collaboration), arXiv:hep-ex/0612034.
[47] M. J. Ramsey-Musolf and S. Su, Phys. Rep. **456**, 1 (2008).
[48] J. R. Ellis, S. Heinemeyer, K. A. Olive, A. M. Weber, and G. Weiglein, J. High Energy Phys. 08 (2007) 083.
[49] P. H. Chankowski and S. Pokorski, in *Perspectives on Supersymmetry*, edited by S. G. L. Kane (World Scientific, Singapore, 1998), pp. 402–422.
[50] J. Alcaraz *et al.* (LEP Collaboration), arXiv:0712.0929.
[51] A. Sirlin, Phys. Rev. D **22**, 971 (1980).
[52] W. J. Marciano and A. Sirlin, Phys. Rev. D **22**, 2695 (1980).
[53] S. Heinemeyer, W. Hollik, A. M. Weber, and G. Weiglein, J. High Energy Phys. 04 (2008) 039.
[54] S. Heinemeyer, W. Hollik, D. Stockinger, A. M. Weber, and G. Weiglein, J. High Energy Phys. 08 (2006) 052.
[55] See the CERN Yellow Book, CERN Report No. CERN 95-03.
[56] ALEPH Collaboration, Phys. Rep. **427**, 257 (2006).
[57] G. W. Bennett *et al.* (Muon G-2 Collaboration), Phys. Rev. D **73**, 072003 (2006).
[58] M. Davier, Nucl. Phys. B, Proc. Suppl. **169**, 288 (2007).
[59] K. Hagiwara, A. D. Martin, D. Nomura, and T. Teubner, Phys. Lett. B **649**, 173 (2007).

[60] D. W. Hertzog, J. P. Miller, E. de Rafael, B. Lee Roberts, and D. Stockinger, arXiv:0705.4617.
[61] D. Stockinger, arXiv:0710.2429.
[62] J. P. Miller, E. de Rafael, and B. L. Roberts, Rep. Prog. Phys. **70**, 795 (2007).
[63] D. Stockinger, J. Phys. G **34**, R45 (2007).
[64] G. Belanger, F. Boudjema, A. Pukhov, and A. Semenov, Comput. Phys. Commun. **180**, 747 (2009).
[65] G. Belanger, F. Boudjema, A. Pukhov, and A. Semenov, Comput. Phys. Commun. **176**, 367 (2007).
[66] G. Belanger, F. Boudjema, A. Pukhov, and A. Semenov, Comput. Phys. Commun. **174**, 577 (2006).
[67] G. Belanger, F. Boudjema, A. Pukhov, and A. Semenov, Comput. Phys. Commun. **149**, 103 (2002).
[68] S. Marchetti, S. Mertens, U. Nierste, and D. Stockinger, Phys. Rev. D **79**, 013010 (2009).
[69] M. Davier *et al.*, Eur. Phys. J. C **66**, 127 (2010).
[70] S. Schael *et al.* (ALEPH Collaboration) Eur. Phys. J. C **47**, 547 (2006).
[71] M. Wick and W. Altmannshofer, AIP Conf. Proc. **1078**, 348 (2008).
[72] M. Misiak *et al.*, Phys. Rev. Lett. **98**, 022002 (2007).
[73] M. Misiak, arXiv:hep-ph/0609289.
[74] M. Misiak and M. Steinhauser, Nucl. Phys. **B764**, 62 (2007).
[75] P. Gambino and P. Giordano, Phys. Lett. B **669**, 69 (2008).
[76] E. Barberio *et al.* [Heavy Flavor Averaging Group (HFAG) Collaboration], arXiv:0704.3575.
[77] F. Mahmoudi, Comput. Phys. Commun. **178**, 745 (2008).
[78] G. Degrassi, P. Gambino, and P. Slavich, Comput. Phys. Commun. **179**, 759 (2008).
[79] A. J. Buras, Phys. Lett. B **566**, 115 (2003).
[80] T. Aaltonen *et al.* (CDF Collaboration), Phys. Rev. Lett. **100**, 101802 (2008).
[81] We thank C. S. Lin for providing us with the likelihoods.
[82] A. Abulencia *et al.* (CDF Collaboration), Phys. Rev. Lett. **97**, 242003 (2006).
[83] M. Bona *et al.* (UTfit Collaboration), J. High Energy Phys. 10 (2006) 081.
[84] G. Isidori and P. Paradisi, Phys. Lett. B **639**, 499 (2006).
[85] M. R. Ahmady and F. Mahmoudi, Phys. Rev. D **75**, 015007 (2007).
[86] E. Komatsu *et al.* (WMAP Collaboration) Astrophys. J. Suppl. Ser. **180**, 330 (2009).
[87] M. Verzocchi, in talk at ICHEP, Philadelphia, PA, 2008.
[88] T. Moroi, Phys. Rev. D **53**, 6565 (1996).
[89] G. Degrassi and G. F. Giudice, Phys. Rev. D **58**, 053007 (1998).
[90] S. Heinemeyer, D. Stockinger, and G. Weiglein, Nucl. Phys. **B690**, 62 (2004).
[91] S. Heinemeyer, D. Stockinger, and G. Weiglein, Nucl. Phys. **B699**, 103 (2004).
[92] T. Becher and M. Neubert, Phys. Rev. Lett. **98**, 022003 (2007).
[93] G. Isidori, F. Mescia, P. Paradisi, and D. Temes, Phys. Rev. D **75**, 115019 (2007).
[94] A. G. Akeroyd and S. Recksiegel, J. Phys. G **29**, 2311 (2003).
[95] B. Aubert *et al.* (*BABAR* Collaboration), Phys. Rev. Lett. **95**, 041804 (2005).
[96] P. Chang, in talk at ICHEP, Philadelphia, PA, 2008.
[97] A. Gray *et al.* (HPQCD Collaboration), Phys. Rev. Lett. **95**, 212001 (2005).
[98] J. F. Grivaz, in *Perspectives on Supersymmetry*, edited by G. L. Kane (World Scientific Publishing Company, Singapore, 1998).
[99] F. Abe *et al.* (CDF Collaboration), Phys. Rev. D **46**, R1889 (1992).
[100] V. M. Abazov *et al.* (D0 Collaboration), Phys. Rev. Lett. **102**, 161802 (2009).
[101] P. Skands *et al.*, J. High Energy Phys. 07 (2004) 036.
[102] F. Feroz, M. P. Hobson, L. Roszkowski, R. R. de Austri, and R. Trotta, arXiv:0903.2487.
[103] R. Barbieri and A. Strumia, arXiv:hep-ph/0007265.
[104] J. A. Casas, J. R. Espinosa, and I. Hidalgo, J. High Energy Phys. 01 (2004) 008.
[105] S. Cassel, D. M. Ghilencea, and G. G. Ross, Nucl. Phys. **B825**, 203 (2010).
[106] J. Kasahara, K. Freese, and P. Gondolo, Phys. Rev. D **79**, 045020 (2009).
[107] R. Barbieri and G. F. Giudice, Nucl. Phys. **B306**, 63 (1988).
[108] G. L. Kane and S. F. King, Phys. Lett. B **451**, 113 (1999).
[109] V. Barger *et al.*, Phys. Rev. D **75**, 115002 (2007).
[110] L. Roszkowski, R. Ruiz de Austri, R. Trotta, Y.-L. S. Tsai, and T. A. Varley, arXiv:0903.1279.
[111] T. Stefaniak, arXiv:0806.2214.
[112] K. Griest and D. Seckel, Phys. Rev. D **43**, 3191 (1991).
[113] J. Edsjo and P. Gondolo, Phys. Rev. D **56**, 1879 (1997).
[114] D. Hooper and E. A. Baltz, Annu. Rev. Nucl. Part. Sci. **58**, 293 (2008).
[115] J. Angle *et al.* (XENON Collaboration), Phys. Rev. Lett. **100**, 021303 (2008).
[116] D. S. Akerib *et al.* (CDMS Collaboration), Phys. Rev. Lett. **96**, 011302 (2006).
[117] D. S. Akerib *et al.* (CDMS Collaboration), Phys. Rev. D **73**, 011102 (2006).
[118] G. J. Alner *et al.*, Astropart. Phys. **28**, 287 (2007).
[119] G. J. Alner *et al.* (UK Dark Matter Collaboration), Astropart. Phys. **23**, 444 (2005).
[120] V. Sanglard *et al.* (The EDELWEISS Collaboration), Phys. Rev. D **71**, 122002 (2005).
[121] G. Angloher *et al.*, Astropart. Phys. **23**, 325 (2005).
[122] P. Benetti *et al.*, Astropart. Phys. **28**, 495 (2008).
[123] R. Brunetti *et al.* (WARP Collaboration), New Astron. Rev. **49**, 265 (2005).
[124] W. J. Bolte *et al.*, J. Phys. Conf. Ser. **39**, 126 (2006).
[125] E. I. Gates, G. Gyuk, and M. S. Turner, Phys. Rev. D **53**, 4138 (1996).
[126] E. Gates, G. Gyuk, and M. S. Turner, arXiv:astro-ph/9704253.
[127] A. K. Drukier, K. Freese, and D. N. Spergel, Phys. Rev. D **33**, 3495 (1986).
[128] R. Bernabei *et al.*, arXiv:astro-ph/0311046.
[129] G. Jungman, M. Kamionkowski, and K. Griest, Phys. Rep. **267**, 195 (1996).
[130] G. B. Gelmini, P. Gondolo, and E. Roulet, Nucl. Phys.

B351, 623 (1991).
[131] M. Srednicki and R. Watkins, Phys. Lett. B **225**, 140 (1989).
[132] M. Drees and M. Nojiri, Phys. Rev. D **48**, 3483 (1993).
[133] M. Drees and M. M. Nojiri, Phys. Rev. D **47**, 4226 (1993).
[134] J. R. Ellis, A. Ferstl, and K. A. Olive, Phys. Lett. B **481**, 304 (2000).
[135] A. Bottino, F. Donato, N. Fornengo, and S. Scopel, Astropart. Phys. **18**, 205 (2002).
[136] A. Bottino, F. Donato, N. Fornengo, and S. Scopel, Astropart. Phys. **13**, 215 (2000).
[137] J. R. Ellis, K. A. Olive, Y. Santoso, and V. C. Spanos, Phys. Rev. D **71**, 095007 (2005).
[138] A. Arbey and F. Mahmoudi, Phys. Lett. B **669**, 46 (2008).
[139] V. Barger, D. Marfatia, and A. Mustafayev, Phys. Lett. B **665**, 242 (2008).
[140] D. S. Sivia and J. Skilling, *Data Analysis—A Bayesian Tutorial* (Oxford Science Publications, Oxford, U.K., 2006), 2nd ed.
[141] D. Feldman, Z. Liu, and P. Nath, J. High Energy Phys. 04 (2008) 054.
[142] C. Balazs and D. Kahawala, arXiv:0904.0128.
[143] N. Metropolis, A. W. Rosenbluth, M. N. Rosenbluth, A. H. Teller, and E. Teller, J. Chem. Phys. **21**, 1087 (1953).
[144] F. Feroz, P. J. Marshall, and M. P. Hobson, arXiv:0810.0781.
[145] F. Feroz, M. P. Hobson, J. T. L. Zwart, R. D. E. Saunders, and K. J. B. Grainge, arXiv:0811.1199.
[146] R. Trotta, F. Feroz, M. P. Hobson, L. Roszkowski, and R. Ruiz de Austri, J. High Energy Phys. 12 (2008) 024.